Universität Hamburg
DER FORSCHUNG | DER LEHRE | DER BILDUNG

FAKULTÄT
FÜR MATHEMATIK, INFORMATIK
UND NATURWISSENSCHAFTEN

Observational Evidence for High Cloud Changes with Changing Surface Temperature

Master thesis
by
Friederike Bär

Studiengang M.Sc. Meteorologie
MIN-Fakultät
Universität Hamburg
November 2019

1^{st} Supervisor: Prof. Dr. Stefan Bühler
2^{nd} Supervisor: Dr. Ákos Horváth

Topic: Observational Evidence for High Cloud Changes with Changing Surface Temperature

Abstract

Since clouds play a significant role in the earths energy budget it is important to know their behavior within a warming climate. One theory for changes of high clouds in the tropics is that they rise due to surface warming and therefore account for a positive cloud feedback. While the fixed anvil temperature hypothesis (Hartmann and Larson, 2002) argues that the detrainment level of high clouds rises isothermally, the proportional higher anvil temperature hypothesis (PHAT) (Zelinka and Hartmann, 2010) shows that an increase in static stability leads to a slight warming of cloud tops, reducing the strength of the feedback. Furthermore, the stability iris hypothesis (Bony et al., 2016) claims that the increase in static stability leads to a reduction of the horizontal high cloud extent.

Many aspects of these theories have been investigated with climate models, however only a limited number of studies exist that examine these mechanisms with observational data. Hence, the aim of this study is to find evidence for the rise of high clouds due to surface warming in observational data and determine to what degree the proposed mechanisms represent reality. The satellite dataset CLARA-A2 is used to construct a cloud top fraction profile, which is compared to a convergence profile generated with the radiative-convective equilibrium model konrad, similar to method of Zelinka and Hartmann (2011). It is shown that anvil cloud height and sensitivity to surface warming coincide well with peaks of convergence. As a response to a surface warming the convergence and cloud top fraction peak slightly shifts to greater heights. Due to considerable uncertainties, it is not clear whether the shift is isothermal, but a PHAT-like response is more likely. In addition, a strong relationship between convergence and static stability is found, which could indicate a stability iris effect, however a link to surface temperature changes is not evident.

Contents

List of Figures

List of Tables

1 Introduction

The Earth's radiation budget is strongly affected by clouds, since they restrict the emission of thermal radiation to space and reflect solar radiation back to space. These effects are highly sensitive to the vertical distribution of clouds. One strong contributor to longwave radiaitve effects are tropical anvil clouds, as they cover large areas in the upper tropical troposphere. Thus it is important to know how tropical anvil clouds respond to a warming planet in order to estimate the strength of the cloud feedback.

One prominent finding in several climate models and observational studies is that high anvil clouds in the tropics tend to rise almost isothermally as the climate warms. This accounts for a positive cloud feedback, since the atmosphere becomes less effective at radiating heat away to space. This mechanism is called fixed anvil temperature (FAT) hypothesis and was developed by Hartmann and Larson (2002). They claim that the behavior of tropical anvil clouds within a changing climate can be expressed with the simple physics of the Clausius Clapeyron relationship. Since water vapor saturation depends exclusively on temperature, the temperature where water vapor becomes inefficient for radiative cooling in the upper troposphere will stay approximately constant. Above this height radiative cooling decreases rapidly and induces strong diabatic convergence. Assuming a closed mass budget, convergence in clear-sky regions must be equivalent to divergence in the convective regions, leading to the formation of anvil clouds. Thus, the diabatic convergence is a strong tool for diagnosing the height of high anvil clouds and their upward shift.

In contrast, Zelinka and Hartmann (2010) showed that the peak in the upper tropospheric convergence shifts to warmer temperatures as the climate warms due to an increase in static stability, and as a result the anvil temperature does in fact increase in model simulations. Therefore the FAT hypothesis was adapted to the proportionally higher anvil temperature (PHAT) hypothesis. To confirm model results, Zelinka and Hartman (2011) tested the PHAT mechanism with observational and reanalysis data. They compared altitude and fractional cloud coverage of several satellite observations with upper tropospheric convergence computed from the energy and mass balance in the tropics. Zelinka and Hartmann (2011) found the observations to be largely in agreement with climate models that clouds rise while staying at nearly the same temperature as the surface temperature warms, thereby suggesting a PHAT-like respond.

Besides the mechanisms involving a vertical displacement of clouds, there are also theories for changes in the horizontal cloud extent. One of the earliest contributions considering the horizontal changes in high clouds is the iris hypothesis by Lindzen et al. (2001), which predicts that the fraction of anvil clouds decreases as the surface warms, thereby acting as a negative cloud feedback by reducing inhibition of longwave radiation from the surface to space. A newer interpretation of the iris hypothesis was provided by Bony et al. (2016). This study shows that a reduction of anvil cloud fraction is caused by the more stable upper troposphere with global warming. This stability iris effect differs to the iris effect first proposed by Lindzen et al. (2001), which focuses on microphysical mechanisms.

There is still some considerable uncertainty surrounding the response of high clouds to global warming, not least because there is limited support for changes in high clouds by observational studies (IPCC, 2013). Hence the aim of this study is to extend the observational evidence for changes in high clouds and investigate to what extent high clouds change according to the FAT, PHAT and iris hypotheses. This is conducted by following the method of Zelinka and Hartmann (2011) evaluating to what degree high cloud variability is due to variations of the surface temperature and thereby validating the method. The observational data chosen for the study are the cloud top properties from the CLARA-A2 satellite dataset and the HadCRUT4 surface temperature dataset. Following Zelinka and Hartmann (2011), diabatic convergence is calculated from the radiative-convective equilibrium, using the radiative-convective equilibrium model konrad (Kluft and Dacie, 2019) with temperature and specific humidity profiles from ERA5 as input. The diabatic convergence profile is compared to observational cloud fraction profile generated from the CLARA-A2 cloud top pressure. The same regression analysis as Zelinka and Hartmann (2011) is conducted in order to understand the sensitivity to surface warming. Finally it is investigated whether the resulting perturbation profiles of convergence and cloud top fraction support to the FAT, PHAT or iris hypothesis.

The outline of this study is as follows. Chapter 2 provides a description of the theoretical background, including more detailed descriptions of the formation of anvil clouds and the theory on how they will react to a warming climate. The data, the radiative transfer model as well as the methods used throughout the analysis are presented in Chapter 3. After that the results are presented in Chapter 4 and the study is summarized and concluded in Chapter 5.

2 Background

The energy flows in and out of the earths atmosphere are highly important for earth's temperature. The earth receives most of its energy by shortwave radiation from the sun. Assuming the earth as an ideal black body, the surface radiates the same amount of energy back to space in the form of longwave radiation (Hartmann, 2015). However, the earth is no ideal black body, since clouds and gases in the atmosphere highly influence this energy balance. At least 50% of the atmosphere are covered by clouds (Liou, 2002). Depending on their horizontal extent, vertical position, thermodynamic phase, liquid or ice content and on their particle size distribution clouds trap longwave radiation from the surface and reflect solar radiation back to space (Liou, 2002). The more clouds are in the atmosphere the more solar radiation is reflected back to space leading to a cooling of the surface temperature. In contrast, clouds absorb longwave radiation from the atmosphere and surface below them and usually emit at colder temperatures than the surface, inducing a reduction of emitted longwave radiation to space, which has a warming effect. The higher and colder the cloud tops are, the more ineffective they are in emitting radiation to space, and thus the more effective they are at warming the surface and atmosphere below. Combining theses effects the net global mean cloud radiative effect is approximately $-20\,Wm^{-2}$ accounting for a strong net cooling effect of clouds in the current climate (IPCC AR5, 2013).

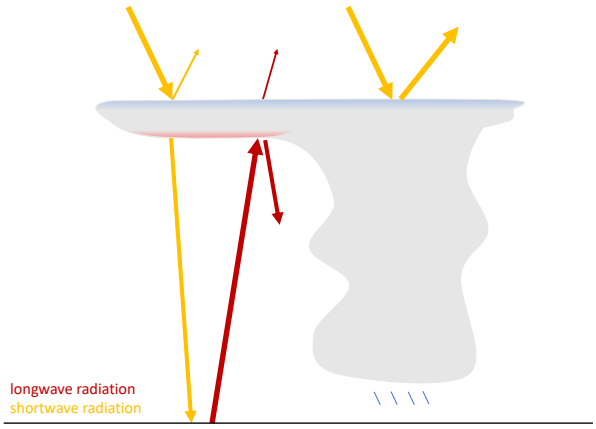

Figure 2.1: Radiative effects of tropical anvil clouds. The cloud base is strongly heated, since more longwave radiation from the surface is absorbed, than downward radiation from the cloud base is emitted. Cooling at the top by emitting infrared emission to space. Strong cooling in region of convective core, because of higher optical thicknesses.

In the tropics the solar radiation strongly heats the ocean and this energy must be removed from the surface. An effective mechanism is moving the energy upward into the free troposphere where the energy can be transported pole-wards and eventually emitted to space (Hartmann, 2016). This upward motion results in the formation of convective cloud systems. These normally are cumulonimbus clouds with a cirri-form cloud shield near the tropopause, often called anvil cloud. Compared to the area covered by the convective cloud tower, the area of anvil clouds is significantly larger, making anvil clouds more important for the earth's radiative energy balance (Hartmann, 2016).

Anvil clouds are mainly composed of ice crystals and therefore they are less reflective for sunlight, than liquid clouds (Schönwiese, 2008). Furthermore, because of their cold cloud top, they are less effective at emitting radiation to space than other clouds, thus they trap more longwave radiation. These effects are strongly sensitive to the height and amount of the clouds. If the clouds rise, the downward infrared flux is enhanced and increasing in cloud amount leads to more trapped longwave radiation. Therefore anvil clouds play an important role for the longwave cloud radiative effect.

2.1 Formation of Anvil Clouds

The formation of anvil clouds in the tropics can be illustrated with the concept of the radiative-convective equilibrium (Manabe and Strickler, 1964). The radiative-convective equilibrium assumes that that the tropical troposphere consists out of two regions: The convective and the clear-sky regions. In the clear-sky regions the troposphere is cooled by radiative cooling and this cooling is balanced by adiabatic heating associated with vertical downward motion. In the convective region the atmosphere is heated by the release of latent heat, causing the air to rise and leading to the formation of convective clouds. These two regions are coupled through a large-scale mass conserving circulation and are approximately in balance (Hartmann and Larson, 2002). This implies that it is only possible to heat the troposphere by convection where it is cooled by radiation (Zelinka and Hartmann, 2010). Hence the altitude level where clouds occur is limited by the appearance of radiative cooling.

The strongest contributor to radiative cooling in the troposphere is water vapour (Liou, 2002), which is mainly controlled by temperature. The dependence of water vapour saturation pressure on temperature is given by the Clausius Clapeyron relationship:

$$\frac{de_s}{dT} = \frac{L}{R_v T^2} e_s \tag{2.1}$$

and can be rewritten as :

$$\frac{dlne_s}{dT} = \frac{L}{R_v T^2} \tag{2.2}$$

and follows the conclusion that the fractional rate of change of the saturation vapor pressure, which gives the limit for the maximum amount of water vapour, exclusively depends on temperature. R_v is the gas constant for water vapour and L is the latent heat of evaporation. Water vapour increases by about 7% for each degree warming of the surface temperature (Hartmann, 2015).

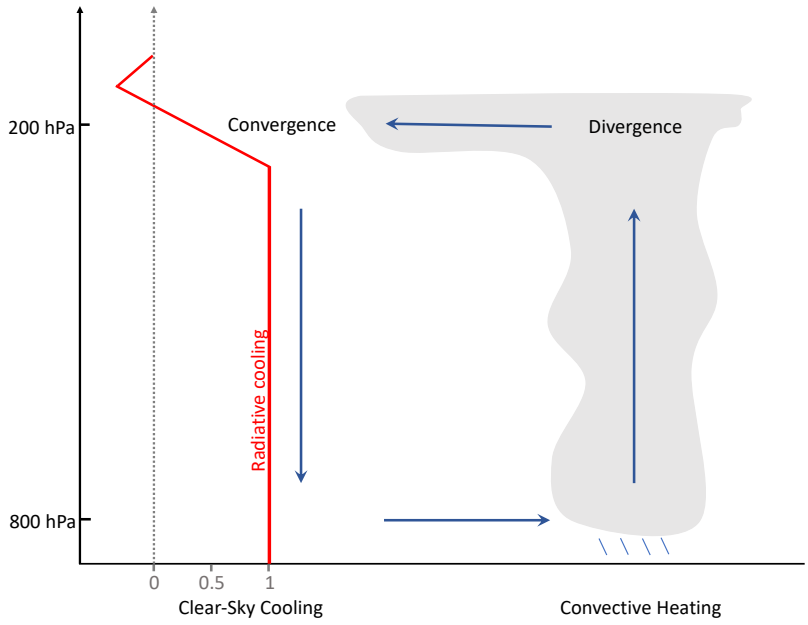

Figure 2.2: Schematic showing of the relation between convective heating and clear-sky cooling.

At certain heights in the upper troposphere the amount of water vapor becomes too low for effectively emitting longwave radiation, causing a rapid decline in radiative cooling. Hence, subsidence declines, causing a strong horizontal convergence. In order to obtain the mass balance, the convergence in the clear-sky region must be accompanied by a strong horizontal divergence in the convective region, which leads to the formation of anvil clouds. Therefore the level of peak convergence should correspond to the height of anvil clouds which has been confirmed by several studies with modeled or observational data (Zelinka and Hartmann (2010), Zelinka and Hartmann (2011), Kuang and Hartmann (2007)). The study by Bony et al. even demonstrates that there is a near linear relationship between diabatic convergence and

anvil cloud fraction. Also Kubar et al. (2007) demonstrate that there is a linear relationship between anvil cloud top temperature and temperature of the maximum convergence.

2.2 Thermodynamic background

Since the diabatic convergence in the clear sky region is of central importance for the formation of anvil clouds, an expression will be derived in the following. This is done by starting with the thermodynamic energy equation. Following Thompson et al. (2017) the thermodynamic energy equation for a steady state in pressure coordinates can be written as

$$\boldsymbol{V} \cdot \nabla_h T - \omega s = Q, \tag{2.3}$$

where the first term on the left-hand site denotes the horizontal advection of temperature, ω the vertical velocity in pressure coordinates, s the static stability and Q represents the heating caused by diabatic processes. Considering only the tropical regions the horizontal advection of temperature is neglectable ($|V \cdot \nabla_h T| \sim 0$) due to very small temperature differences. Hence, the vertical motion is given by

$$\omega = -\frac{Q}{s}, \tag{2.4}$$

with the static stability as

$$s = -\frac{T}{\theta}\frac{\partial \theta}{\partial p} = -\frac{T}{p} + \frac{R_d}{c_p}\frac{T}{p}, \tag{2.5}$$

where θ is the potential temperature, R_d the gas constant for dry air and c_p the specific heat at constant pressure. Following equation 2.4 vertical motion is balanced by heating due to diabatic processes. In the clear-sky regions the most dominant process is radiative cooling by water vapour. Saying that radiative cooling is balanced by adiabatic heating induced by subsidence. Retaining the assumptions of mass continuity in the tropics the diabatic convergence profile can be expressed as

$$-\nabla_H \cdot \boldsymbol{U} = \frac{\partial w}{\partial p}, \tag{2.6}$$

where the left term is the horizontal convergence. Assuming mass continuity between convective and clear-sky region, the convergence must be mimicked by diabatic divergence in the convective regions. With this system of equations the level of convective detrainment can be easily calculated and no additional processes like parcel entrainment or complex moist physics need to be considered.

2.3 Sensitivity to Surface Temperature changes

Since clouds in the current climate have a strong net cooling effect, it is of major interest to know how they behave in a warming climate. In general, changes in clouds related to global warming are referred to as the cloud climate change feedbacks, in short cloud feedbacks. The magnitude of the net cloud feedback in all global climate models used in the Assessment Report 5 (IPCC (2013)) is generally positive, as they strengthen the warming. However, the intermodel spread illustrates that the cloud feedback is a major source for uncertainties for estimating earth's sensitivity to global warming (Bony et al., 2006). Hence, it is essential to improve the understanding of cloud feedbacks in order to reduce uncertainties.

The uncertainties related to the long wave cloud feedback have been somewhat reduced recently. Zelinka and Hartmann (2010) demonstrated that the longwave cloud feedback is robustly positive at 0.5 $Wm^{-2}K^{-1}$ comparing twelve global climate models, which is caused by the tendency of high clouds to rise in a warming climate. The mechanisms behind the proposed rise in high clouds are described by the FAT/PHAT hypothesis, while changes in horizontal extent are described by the IRIS effect. These three theories will be explained in the following.

2.3.1 Fixed Anvil Temperature (FAT) Hypothesis

As high clouds strongly contribute to longwave radiative effect, changes in high clouds mainly determine the longwave cloud feedback. One theory for changes in anvil clouds is the Fixed Anvil Temperature Hypothesis (FAT) by Hartmann and Larson (2002). The FAT hypothesis states, that the temperature where water vapor becomes inefficient for radiative cooling will stay approximately constant during global warming and thus also the cloud top temperature of anvil clouds. As the surface temperature increases in a warming climate, the whole troposphere warms, this implies that also the amount of water vapor increases. Hence the temperature where water vapour cooling becomes inefficient shifts upwards due to rising isotherms. This leads to a upward shift of the peak convergence, which must be mimicked by the divergence in the convective regions. Therefore the level of anvil clouds rises as well and the cloud top temperature stays fixed. This results in a positive longwave cloud feedback, as the clouds are not warming at the same rate as the surface making the tropics less efficient in radiating heat away, according to the Planck law. Various studies have tested the FAT hypothesis and most have found supporting evidence for it. Making use of cloud-resolving simulations for a restricted area, Kuang and Hartmann (2007) finds evidence that the cloud top temperature of anvil clouds changes less than $0.5K$ for a surface warming of

$2K$. In addition, they show that other changes in the model setup for example changes in stratospheric water vapour concentration or changes in CO_2 mixing ratio have no influence on the temperature. Eitzen et al. (2009) and Xu et al. (2005, 2007) analyzed cloud top temperature measured by the CERES instrument on board of the Tropical Rainfall Measuring Mission (TRMM) satellite. Xu et al. focused on cloud tops greater than 100km equivalent diameter, which occurred during El Niño 1998. For cloud tops larger then 300km the cloud top temperature stayed nearly constant during surface temperature variations. Also Eitzen et al. demonstrated that the cloud top is invariant to surface temperature changes related to El Niño 1998. The analysis was restricted to deep convective systems with cloud top heights higher than $10km$ and a threshold of 10 for the optical thickness. All theses results demonstrate that there is a high likelihood for the fixed anvil temperature hypothesis to present the actual behavior of high clouds.

2.3.2 Proportional Higher Anvil Temperature (PHAT) Hypothesis

In contrast to the FAT hypothesis, Zelinka and Hartmann (2010) demonstrates that the anvil cloud top temperature slightly warms in a warming climate. Using the the climate models used in the Intergovernmental Panel on Climate Change Fourth Assessment Report (AR4) they investigated why the longwave cloud feedback in these climate models is smaller than the cloud feedback would be assuming the anvil cloud temperature stays fixed. The results demonstrate that the tropical high clouds shift upwards as the climate warms. However, this upward shift is accompanied by a very modest increase in cloud top temperature, which reduces the negative longwave cloud feedback. As the surface warms the temperature of the level of maximum diabatic convergence warms and therefore the anvil cloud top temperature warms as well. The static stability increases proportional to temperature and therefore reduces the diabatic subsidence resulting in a reduction and shift to slightly warmer temperatures of the diabatic convergence maximum. This is mimicked in a decrease and slightly warming of the anvil clouds. Therefore Zelinka and Hartmann adapted the FAT hypothesis to Proportional Higher Anvil Temperature (PHAT). The cloud tops slightly warm and the longwave cloud feedback is still positive, however slightly smaller than assuming FAT. Support for the PHAT hypothesis is provided by Harrop and Hartmann (2012). A cloud-resolving model is used to demonstrate a slight increase in anvil cloud top temperature for an increase in surface temperature. This is caused by an enhanced static stability in the upper troposphere. Furthermore it is shown, that radiative effects of ozone, carbon-dioxide and clouds are less important for changes in static stability than the effects of water vapor. Chae and Sherwood (2010) found evidence for a connection between stability and height of tropical anvil clouds as well, us-

ing cloud top measurements from the Multi-angle Imaging Spectroradiometer (MISR) for the specific region of the western Pacific Ocean. It is illustrated that the mixing between overshooting convection and environment, where stability is highly important, could represent one mechanism that connects stability and anvil heights. Using MODIS, CloudSat, ISCCP and CERES satellite measurements Zelinka and Hartmann (2011) show, that for a surface warming of $1K$, due to ENSO events, the convergence peak shifts to slightly warmer temperatures, which is accompanied by an increase in static stability. This shift to warmer temperatures is also seen for the cloud top temperature implying to a PHAT-like response. The results do not contradict the FAT hypothesis, however these studies illustrates that other parameters influencing the cloud top height, like static stability, should not be overlook. Therefore the improved FAT hypothesis PHAT is more similar to what can be observed and therefore likely closer to reality.

2.3.3 Iris Hypothesis

The FAT and PHAT mechanisms described above deal with the vertical displacement of the avail clouds. However, there have also been suggestions as to how anvil clouds could change in their horizontal extent in a warming climate. One possibility is the Iris hypothesis a theory proposed by Lindzen et al.. The hypothesis claims, that in a warmer climate the precipitation efficiency is enhanced, leading to a reduction of anvil clouds, which are detrained to the troposphere by convection. The decline in cloud cover lets more infrared radiation escape to space reducing the warming effects of anvil clouds. This would account for a negative longwave cloud feedback. Similar to the way a human eye's iris opens and closes depending on the light level, the anvil cloud cover can change to control the outgoing longwave radiation to space as a response to changing surface temperatures. However, several studies demonstrated that there are a few physical problems with this hypothesis (Hartmann and Michelsen (2002), Lin et al. (2002)). It is argued that the method and definitions of Lindzen et al. are not completely correct and clear. The study by Mauritsen and Stevens also tested the Iris hypothesis and shows, that a reduction in cloud cover would indeed cause a negative long wave cloud feedback. However, the positive shortwave feedback from a decreasing anvil cloud cover counteracts the negative longwave feedback, resulting in a slight positive cloud feedback. A new interpretation of the iris effect is presented by Bony et al.. Using general circulation models it is demonstrated that there is a reduction in anvil cloud fraction for warmer surface temperature. Surface warming induces an increase in static stability, which leads to a reduction in convergence and therefore a reduction in the amount of anvil clouds. These results lead to the proposal of an updated hypothesis, the stability iris hypothesis.

3 Data and Methods

The response of high clouds to surface warming has mainly been studied with climate models, while observational support is limited. Therefore this study tests the sensitivity of high clouds to interannual changes in surface temperature and uses observational datasets for the analysis. In addition, a closer investigation of changes in the monthly means is performed. In the following the data, the radiative transfer model as well as the methods used for this study are described.

3.1 Data

In order to find evidence for variability in high clouds due to changes in surface temperature, like the rise of the cloud top due to surface warming (FAT), in observational data the satellite dataset CLARA-A2 and the surface temperature product HadCRUT4 are chosen for the analysis. Satellite data provides a good spatial and temporal resolution of the whole tropical region and therefore is well suited for this analysis. CLARA-A2 was chosen, since the dataset combines measurements from several satellites and is easily accessible to download. HadCRUT4 consists of measured land and sea surface temperature data and provides one of the longest observational surface temperature records. In addition reanalysis data from ERA5 are used for the calculation of the diabatic convergence, since they offer a good vertical and horizontal resolution. Temperature and specific humidity ERA5 profiles are used to calculate the diabatic convergence using the radiative transfer model konrad.

3.1.1 Cloud, Albedo and Radiation dataset: CLARA-A2

This study makes use of the second edition of CM SAF Clouds, Albedo and Radiation (CLARA-A2) dataset level-2b cloud top product, containing cloud top height, pressure and temperature. The dataset is provided by the Satellite Application Facility on Climate Monitoring (CM SAF), currently hosted at the German Weather Service (DWD), which has the goal of generating a long-term data record from operational meteorological satellites. CLARA-A2 combines cloud, surface albedo and surface radiation measurements performed by the Advanced Very High-Resolution Radiometers (AVHRR) on board of the polar orbiting MetOp-A and -B satellites of the EUMETSAT (European Organisation for the Exploitation of Meteorological Satellites) as well as on board of the polar orbiting NOAA-7 to NOAA-19 satellites of the NOAA (National Oceanic and Atmospheric Administration). The NOAA as well as

the MetOp satellites are in a sun-synchronous orbit and are 833 and 820km above the earth respectively.

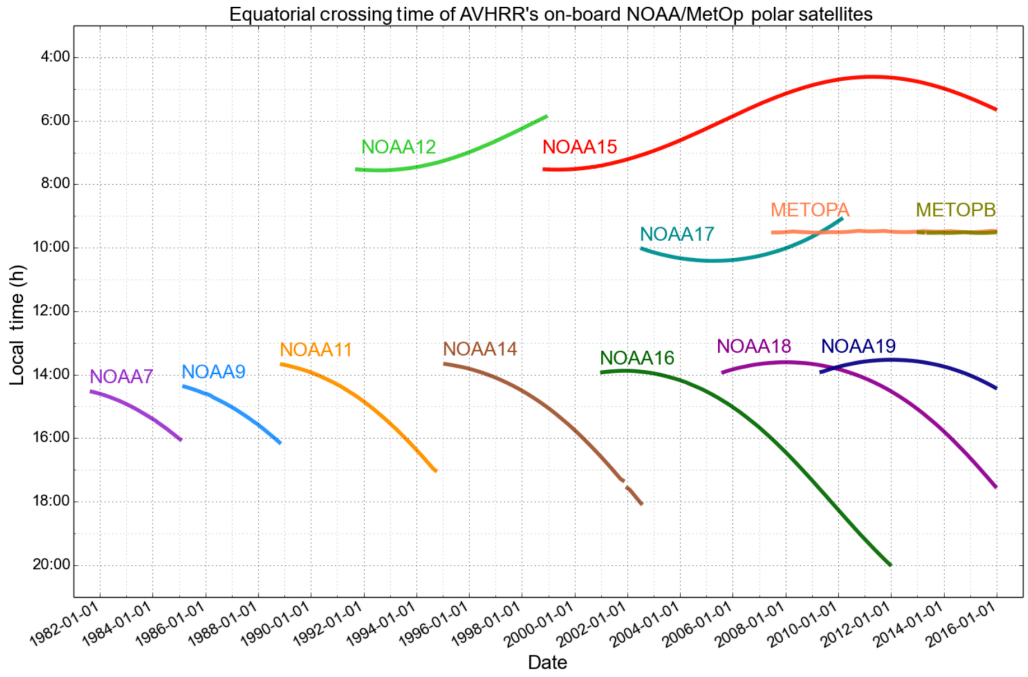

Figure 3.1: Time of equatorial crossing from satellites NOAA-7 to NOAA-19 and MetOp A and B. The corresponding observations for night-time happen 12 hours earlier/later. All observations used for CLARA-A2 are shown.

The earlier AVHRR instruments are four-channel radiometers, while the newer AVHRR instruments, beginning with instruments on board NOAA-15, measure in six spectral channels. A horizontal resolution close to 1km at nadir conditions is provided as well as a global imagery twice a day. The data record of CLARA-A2 starts 1982 and ends 2015, covering a 34-year period. Figure 3.1 illustrates the equatorial crossing time of the different satellites and their respective measurement periods used for the generation of CLARA.

The CLARA data record is global area coverage (GAC) data. The processed data is defined without any overlap in the beginning or in the end of each orbit, so that there are continuous GAC orbits. Orbits with corrupt or incorrect data in the original data are not used for the data processing. Several cloud products are provided, such as the cloud physical, the cloud, mask, the surface albedo, surface radiation and the cloud top product. For this study only cloud top products are used. The measured brightness temperature pixels need to be processed and thereafter averaged to generate daily mean quantities on a regular longitude-latitude grid.

Table 3.1: The six spectral channels of the newer AVHRR instruments. In the beginning only four channels, 1982 a fifth channel was added and finally 1998 a sixth one. Channel 3A was only used continuously on NOAA-17, MetOp-A and MetOp-B.

Channel Number	Wavelength in μm
1	0.58 - 0.68
2	0.725 - 1.10
3A	1.58 - 1.64
3B	3.55 - 3.93
4	10.50 - 11.50
5	11.5 - 12.5

Processing the level-2b Product

Three cloud top products, the cloud top height in units of altitude over ground topography, cloud top pressure in hPa and cloud top temperature in K are available. For deriving these level-2 products one approach for the fractional and semi-transparent clouds and one for the opaque clouds is used. The algorithms are applied to all cloudy pixels, which are detected by the cloud masking method (NWC SAF PPS 2014 version (Karlsson et al., 2016)). The cloud masking method defines cloud fraction cover as fraction of cloudy pixels per grid box compared to the total number of analysed pixels in the grid box (Karlsson et al., 2016). The opaque algorithm compares simulated $11\mu m$ brightness temperatures at the top of the atmosphere for cloudy and cloud free conditions with measured brightness temperatures. The radiances for cloudy conditions are simulated with the EUMETSAT radiative transfer model RTTOV-11 using the ECMWF ERA-Interim profiles, with the assumption that black-body clouds appear at different height-levels. For the semitransparent cirrus or fractional water clouds brightness temperatures between AVHRR channel 3b, 4 and 5 ($3.7\mu m$, $11\mu m$, $12\mu m$) are compared by constructing two dimensional histograms over large spatial boxes. Each box consists out of 12x12 GAC pixels with about $60x60km$. The differences in brightness temperature are usually small for opaque clouds and large for semitransparent clouds. An iterative method is used to produce a polynomial curve, which is fitted to the histogram-plotted values and allowing the cloud top temperature to be retrieved from this curve. The algorithm relies on the assumptions, that the surface temperature typically is significantly warmer than the cloud top temperature and that the transmissivity of ice clouds reduces with increasing wavelength in the infrared.

Further processing of the level-2 product to the level-2b product is necessary, since all polar sun-synchronous satellites together produce an in-homogeneous global coverage. The satellites

provide observations near the pole 14 times a day while they only have 2 observations at the equator per day. For more consistency only two observations per day per satellite for each global location and only observations which are made at nadir condition are taken (Karlsson et al., 2016). This leads to a significant reduction in data, but the observations are weighted correctly. Due to the sampling technique a globally nearly constant number of observations per grid box can be achieved, which helps combining the different satellite datasets. The obtained level-2b product is aggregated to a global regular longitude-latitude grid with a resolution of 0.05°x 0.05° and averaged to daily means (Karlsson et al., 2016).

Processing the level-3 Product

All resampled daily level-2b fields are merged and thereafter weighted by the number of used entries to generate the level-3 dataset. For the level-2b product there are two observations per day per satellite available, which are 12 hours apart. Therefore it is possible that one level-3 grid box consists of 50 level-2b measurements per day depending on the availability of the level-2b measurements. In order to minimize artificial errors due to a lack of data at least two of these level-2b measurements must be available. The final level-3 cloud top product is defined on a regular longitude-latitude grid with a resolution of 0.25°x 0.25° (Karlsson et al., 2017a).

Advantages and Limitations of the Satellite Dataset

Advantages:

- The time range is long and consistent, covering a 34 year period.
- The combination of 12 satellite datasets all measured with the same kind of instrument allows a global coverage with high spatial resolution.
- The data is ready to use, free available and easy to access.

Limitations:

- As seen in Figure 3.1 the orbital drift of a couple of satellites leads to changing local observation times, which changes the observational conditions during the period. This can, for instance, cause trends in the achieved monthly mean products for regions where there is a strong diurnal cycle in cloudiness. There are no correction attempts for this problem in the CLARA-A2 data record.
- The changing availability of satellites leads to some artificial trends in the global cloud cover.

- The AVHRR sensor as a passive radiometer has a relatively coarse field of view. Due to the passive measurement thin clouds with optical thicknesses below 0.15 are not recorded in many cases (Karlsson et al., 2017b). At night-time over desert surfaces sometimes spurious clouds are detected due to problems in estimating surface emissivities. Also mainly in the tropics some overestimation of the cloud fraction (up to 10 %) can be found over some oceanic regions (Karlsson et al., 2017b).

- Apart form these errors related to the measurements itself, several systematic errors are caused by the applied algorithms for cloud screening, as well as detecting the fractional, semi-transparent clouds and the opaque clouds. There are problems at twilight conditions and for strong temperature inversions in the troposphere, leading to systematic underestimations of cloud amount by cloud screening methods. In the case of multi-layered clouds, the brightness temperatures differences are reduced by not measuring the surface, but a lower cloud. Up to 5% cloud fraction may be not detected with the algorithm (Karlsson et al., 2017b) and often the height of thin clouds is underestimated for several kilometers. In addition multi-layer clouds are often interpreted as opaque clouds, which leads to an underestimation of the true cloud top.

There are some further uncertainties which only apply to low clouds and therefore should not impact the results of this study. In summary, CLARA underestimates the height of thin high clouds and overestimates the height of lower clouds, as well as the cloud amount, especially over tropical oceans.

CLARA-A2 compared to MODIS

Due the fact that the CLARA-A2 has some limitations and uncertainties the level-2b and level-3 cloud top pressure are compared to one month of the moderate resolution imaging spectroradiometer (MODIS) cloud top pressure with a resolution of 1°x 1°. The MODIS is on board of the NASA Earth Observing System EOS-TERRA and EOS-AQUA satellites. It is a scanning radiometer equipped with 36 spectral channels ranging from 0.415 to 14.235 μm. Together they cover the entire earth in two days. For deriving the cloud top parameters for mid- and high-level clouds a CO_2 slicing technique is used in combination with numerical and radiative transfer model input (Borbas and MENZEL (2015)). The cloud top pressure is determined by the difference between radiances measured in the spectral band located in the broad $15\mu m$ CO_2 absorption region to radiance measured in the IR-window bands. Each MODIS band senses a different atmospheric layer. For different cloud pressures these differences are matched to calculated theoretical ratios. Since this method is relatively insensitive to emissivity, the temperature of thin clouds can be sensed more accurately compared to estimates

based ob brightness temperatures alone (Platnick et al., 2003). However, one disadvantage of MODIS is that the temporal resolution is considerably lower than that of CLARA-A2.

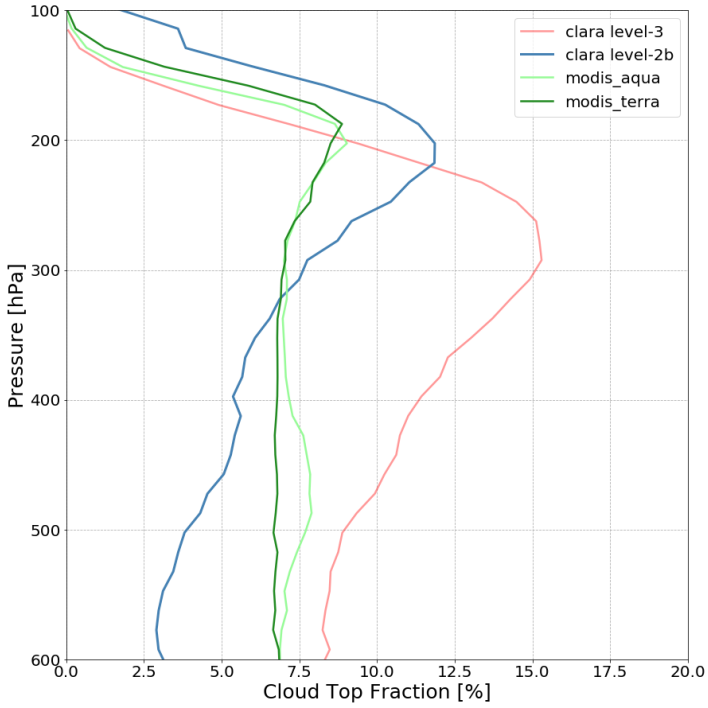

Figure 3.2: Cloud top fraction generated out of the cloud top pressure product of CLARA-A2 level-3 (light-red) and the CLARA-A2 MetOp-A level-2b (blue), with cloud top fraction generated out of MODIS cloud top pressure measurements on board of EOS-Aqua (light-green) and EOS-Terra (dark-green).

In order to check the accuracy of the daily CLARA-A2 level-3 and level-2b (only MetOp-A) product the average of one month of each product is compared to the cloud top product from MODIS. As seen in figure 3.2 the resulting cloud fraction profiles from CLARA level-2b and MODIS agree well with the height of the maximum cloud fraction peak. The peak of CLARA level-2b is at slightly higher pressures. However the cloud amount is larger compared to that of MODIS, which can be caused by the overestimation of the cloud amount over tropical oceans. Furthermore figure 3.2 shows that the cloud top fraction generated with the cloud top pressure of the level-3 product highly underestimates the true height of high clouds and overestimates the cloud amount compared to the cloud top fraction generated with the level-2b data and MODIS data. The CLARA-A2 level-3 product features errors that arise from coarsening the resolution and this merging process is problematic for the resulting cloud top products. Therefore the level-3 product is not suitable for analysing the FAT-mechanism, for which accurate estimates of cloud heights are essential. Also the comparison to MODIS cloud top pressure leads to the conclusion that the CLARA-A2 level-2b product is well suited

for analysing the FAT-mechanism, however the bias in the cloud amount should considered when investigating the IRIS effect. For this reason the daily level-2b product is chosen for the analysis in this study. To further minimise errors only the CLARA-A2 level-2b cloud top product from MetOp-A, which has no orbital drift, is used.

3.1.2 Reanalysis dataset: ERA5

Since the CLARA dataset cannot provide a measure for diabatic convergence, which is needed to validate the FAT mechanism, additional data is necessary. Consequently the reanalysis product ERA5 is used to determine temperature and specific humidity profiles. These profiles are required for the calculation of diabatic convergence using the radiative transfer model konrad. The ERA5 dataset is the fifth generation of reanalysis of the global weather and climate produced by the European Centre for Medium-Range Weather Forecasts (ECMWF) (Hersbach et al., 2019). The reanalysis is available from 1979 until present and is updated every month. A combination of observations and simulation data is assimilated in order to produce a complete and consistent long-term weather and climate record. ERA5 uses 4D-Var data assimilation in a global ensemble system of ECMWFs Integrated Forecast System. The model runs with 137 hybrid sigma/pressure levels in the vertical. The results are interpolated to 37 pressure levels from 1000hPa (surface) to 1hPa (approximately the top of the stratosphere). There are 16 atmospheric quantities available on the pressure levels. For this study monthly temperature and specific humidity profiles, with a spatial resolution of 1° x 1° are used.

3.1.3 Surface temperature anomaly dataset: HadCRUT4

Finally, measurements of the surface temperature are needed to diagnose the sensitivity of high cloud to surface temperature changes. For this study the surface temperature anomalies from HadCRUT4 are chosen. HadCRUT4 is a globally gridded dataset of Surface Temperature Anomalies, originating from collaboration of the Climatic Research Unit at the University of East Anglia and the Met Office Hadley Centre (https://crudata.uea.ac.uk /cru/data/ temperature/). It combines the CRUTEM4 (Climatic Research Unit Temperature) land surface air temperature anomaly dataset with the sea surface temperature anomaly dataset HadSST3 (Hadley Centre Sea Surface Temperature). The data is available as monthly means since 1850, with a 5° spatial resolution. The period between 1961-1990 is used as reference period for calculating the anomalies. Land temperature data originates from over 4800 land stations, with varying distribution around the globe (Morice et al., 2012). For sea temperature measurements of made on board of ships and buoys are used. Therefore the dataset is purely

based on observations.

3.2 Radiative transfer model konrad

The radiative cooling cannot be easily derived from satellite measurements and is also not provided by the ERA5 reanalysis. Therefore, the radiative transfer model konrad (version 0.6.6) by Kluft and Dacie (2019) is necessary for calculating the radiative cooling. The model is based on the clear-sky one-dimensional radiative-convective equilibrium and uses the Rapid Radiative Transfer Model for GCMs (RRTMG) to calculate radiative fluxes. The RRTMG uses the k-correlated scheme in order to accelerate the calculation of fluxes and cooling rates integrated over the full electromagnetic spectrum (Mlawer et al., 1997). In addition, the scheme is edited for the konrad model by using output data from line-by-line models. This allows the calculation of important parts of the electromagnetic spectrum. To check the accuracy of konrad Kluft et al. compared longwave heating rates to the line-by-line transfer model ARTS (Buehler et al. (2018)). The heating rates are calculated for different equilibrium states and have a discrepancy smaller than 0.1 $KDay^{-1}$ in the troposphere.

Model Setup

The model is set up for a slab surface with an albedo of 0.2 and a heat capacity of 215 $MJm^{-2}K^{-1}$, which represents a 50 m deep well-mixed ocean. Furthermore it is set for clear-sky conditions without a diurnal cycle. The solar irradiance is defined as 510 Wm^{-2} and the zenith angel as 47.88°, which results in a incoming shortwave radiation of 342 Wm^{-2} at the top of the atmosphere. Konrad uses the same trace gas concentrations as the Radiative-Convective Equilibrium Model Intercomparison Project (RCEMIP) (Kluft et al., 2019).

Table 3.2: Volume mixing ratios (VMR) of different gases following the RCEMIP configuration (Wing et al.2017)

Gas	Volume mixing ratio	
O_2	21	%
CO_2	348	ppmv
CH_4	1650	ppbv
N_2O	306	ppbv
CO	0	

In addition, the ozone profile, which is calculated as a function of pressure, is fixed. In this study the area-weighted tropical mean temperature and specific humidity profiles from ERA5 are used as input for the model in order to calculate radiative cooling.

3.3 Methods

The methods used for calculating tropical mean profiles and their sensitivity to surface warming are similar to the methods used in the study of Zelinka and Hartmann (2011). In addition, a method for analysing the peaks in upper tropospheric convergence, cloud top fraction and static stability is introduced.

3.3.1 Preparing Tropical Mean Profiles

The tropical mean profiles of temperature and mixing ratio require some preceding preparations before radiative cooling, static stability, diabatic subsidence and diabatic convergence can be calculated.

The ERA5 reanalysis temperature and specific humidity have a relatively coarse vertical resolution of 37 pressure levels. However, a finer vertical resolution improves the accuracy for the determined profiles. Hence both profiles are interpolated logarithmically onto a finer vertical grid. The interpolation was performed with the scipy griddata function using a cubic interpolation[1] for python. The resulting vertical grid has 300 levels between $1000hPa$ and $1hPa$. In addition the specific humidity must be converted into volume mixing ratio, before set as input for the konrad model. The area-weighted tropical mean temperature and volume mixing ratio are used as input for the konrad model in order to calculate the diabatic convergence.
In order to calculate the static stability first the potential temperature must be determined using the ERA5 monthly mean temperature profile. With the potential temperature static stability can be calculated following equation 2.5. The diabatic subsidence is the result of dividing radiative cooling by static stability (equation 2.4). Furthermore the vertical gradient of diabatic subsidence corresponds to diabatic convergence (equation 2.6).

Moist Lapse Rate

Moist adiabatic lapse rates are calculated to characterise the temperature profile. This is done by using the equation for the moist pseudoadiabat (Bakhshaii and Stull, 2013),

$$\frac{dT}{dp} = \frac{1}{p} \frac{R_d T + L_v r_s}{c_{pd} + \frac{L_v^2 r_s \epsilon}{R_d T^2}} \tag{3.1}$$

[1] see https://github.com/scipy/scipy/blob/v1.3.1/scipy/interpolate/ndgriddata.py

with R_d the ideal gas constant for dry air, L_v the latent heat of evaporation, c_{pd} the specific heat at constant pressure for dry air, r_s the saturated mixing ratio and ϵ the ratio of ideal gas constants for dry air and water vapor. Integrating equation 3.1 gives the temperature for a moist adiabatic lifted air parcel.

Cloud top fraction

Since the diabatic convergence must be mimicked by divergence in the convective regions, anvil clouds are formed. Therefore the peak in convergence should be compared to cloud top fraction. Hence a cloud fraction profile is generated by using the daily cloud top pressure fields from the CLARA-A2 MetOp-A level-2b dataset. First the monthly mean of the cloud top pressure is binned into pressure levels, with 15hPa steps between 100 and 1000hPa. The number of entries per bin is normalized, by dividing by the number of entries for the whole month. The resulting frequency is plotted against the geometric mean cloud top pressure for each bin. The corresponding temperature for each pressure bin is found by calculating the geometric mean of cloud top temperature.

Uncertainties

The uncertainties for all tropical profiles are given by their standard deviations.

3.3.2 Sensitivity analysis

In order to investigate the sensitivity to surface warming a regression analysis is performed. The data is prepared by calculating the area weighted monthly means. In the next step the average annual cycle is subtracted of the monthly means to receive the anomalies. A regression coefficient of the monthly anomalies at each pressure level with the surface temperature is calculated:

$$b = \frac{covariance_{x,y}}{variance_x} = \frac{\sum_{i=1}^{n}(x_i - \overline{x})(y_i - \overline{y})}{\sum_{i=1}^{n}(x_i - \overline{x})^2}. \tag{3.2}$$

The calculated regression coefficients correspond to the sensitivity of each quantity to surface temperature changes. For temperature, mixing ratio, radiative cooling, static stability, diabatic subsidence and diabatic convergence the lowest level of the ERA5 temperature profile is used. However, for the observational cloud top fraction the HadCRUT4 surface temperature is used for the regression.

Uncertainties

The uncertainties are estimated using a bootstrapping method. Thus, the monthly anomalies are permuted randomly 10.000 times and each time a new regression coefficient is calculated. The resulting distribution of regression slopes between the 2.5 and 97.5 percentile represents the 95% confidence interval.

3.3.3 Peak analysis

Considering the three possible mechanisms how high cloud are sensitive to changes in surface temperature the variability of cloud top fraction, convergence and static stability is investigated in more detail looking at the monthly mean tropical profiles. One way is by calculating the correlations of cloud top fraction, convergence and static stability at the height of anvil clouds with changes in surface temperature. The maxima of the monthly mean, tropical mean cloud fraction, convergence and static stability are determined for every month along with the according temperature.

Weighted Pressure and Temperature

For a better estimate of the sensitivity to surface warming, high cloud weighted pressure and upper tropospheric clear-sky diabatic convergence weighted pressure are calculated as

$$p_{hicld} = \frac{\sum_{p\,at\,T=270K}^{p\,at\,trop} f\ *\ p}{\sum_{p\,at\,T=270K}^{p\,at\,trop} f}. \tag{3.3}$$

and

$$p_{conv} = \frac{\sum_{p\,at\,T=270K}^{p\,at\,trop} conv\ *\ p}{\sum_{p\,at\,T=270K}^{p\,at\,trop} conv}. \tag{3.4}$$

with f being the high cloud fraction at each pressure. The weighted pressures are calculated for pressures lying between pressures at a temperature of 270K and a temperature at the cold point tropopause. The same weighting is done for temperature resulting in high cloud weighted temperature (T_{hicld}) and upper tropospheric clear-sky diabatic convergence weighted temperature (T_{conv}). This is done by using equation 3.3 and 3.4, where the pressure is substituted with temperature. This method is similar to the calculation by Zelinka and Hartmann (2010).

Regression

For all cases a orthogonal regression of variable x against variable y is performed and shown in a scatter plot. In contrast to the linear regression the orthogonal regression considers error components for both variables and not only one variable. Here the standard deviations for each variable are converted into weights by dividing 1 by the square of the standard deviation to estimate the error.

4 Results

In this section the results of this study are presented, starting with an overview of the tropical climate variations during the analysed time period. The analysis of this study is restricted to the tropical regions, defined as 30° South to 30° North and the time period from beginning of 2008 till the end of 2015. During this period several El Niño Southern Oscillation (ENSO) events occur and strongly influence the surface temperature especially in the central tropical Pacific. ENSO events are associated with unusually large warming (El Niño) or cooling (La Niña) of the sea surface temperature along the coast of Peru and Ecuador occurring every few years, caused by a weakening or strengthening of the trade winds (Trenberth, 1997). This sea surface warming (cooling) propagates westwards in the pacific and influences the whole tropics.

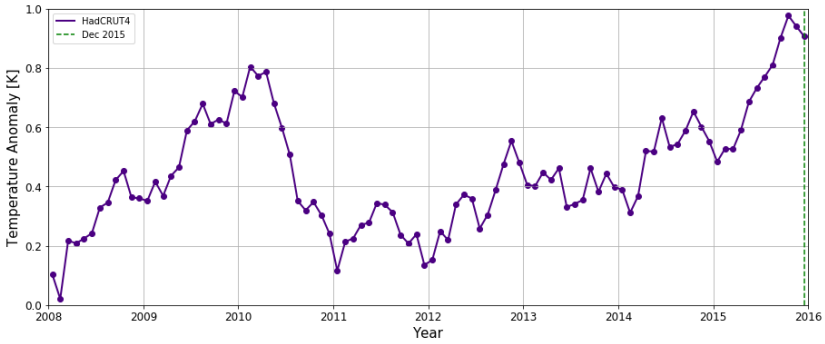

(a) Tropical Monthly Mean Surface Temperature Anomaly

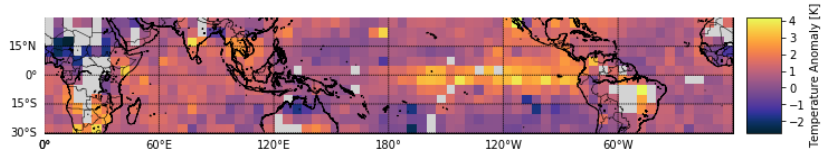

(b) Temperature Anomaly December 2015

Figure 4.1: (a) Tropical monthly mean surface temperature anomalies 2008-2015 from HadCRUT4, with the period of 1961-1990 as reference period. The green line displays December 2015. (b) Monthly mean surface temperature anomalies from HadCURT4 for December 2015.

During this time period the La Niña event in 2008 with quite low temperature anomalies turns into 2010's El Niño, which leads to a steady increase in surface temperature. This is followed by a strong la Niña event 2011 and a moderate event in 2012, again causing a surface cooling. Afterwards the surface temperature warms again due to a weak El Niño event in

2014-2015 and the warming continues until reaching its maximum in 2015 due to a strong El Niño. These temperature differences allow for a sensitivity analysing to varying surface temperature of about $1K$ range.

4.1 Tropical Mean Atmosphere

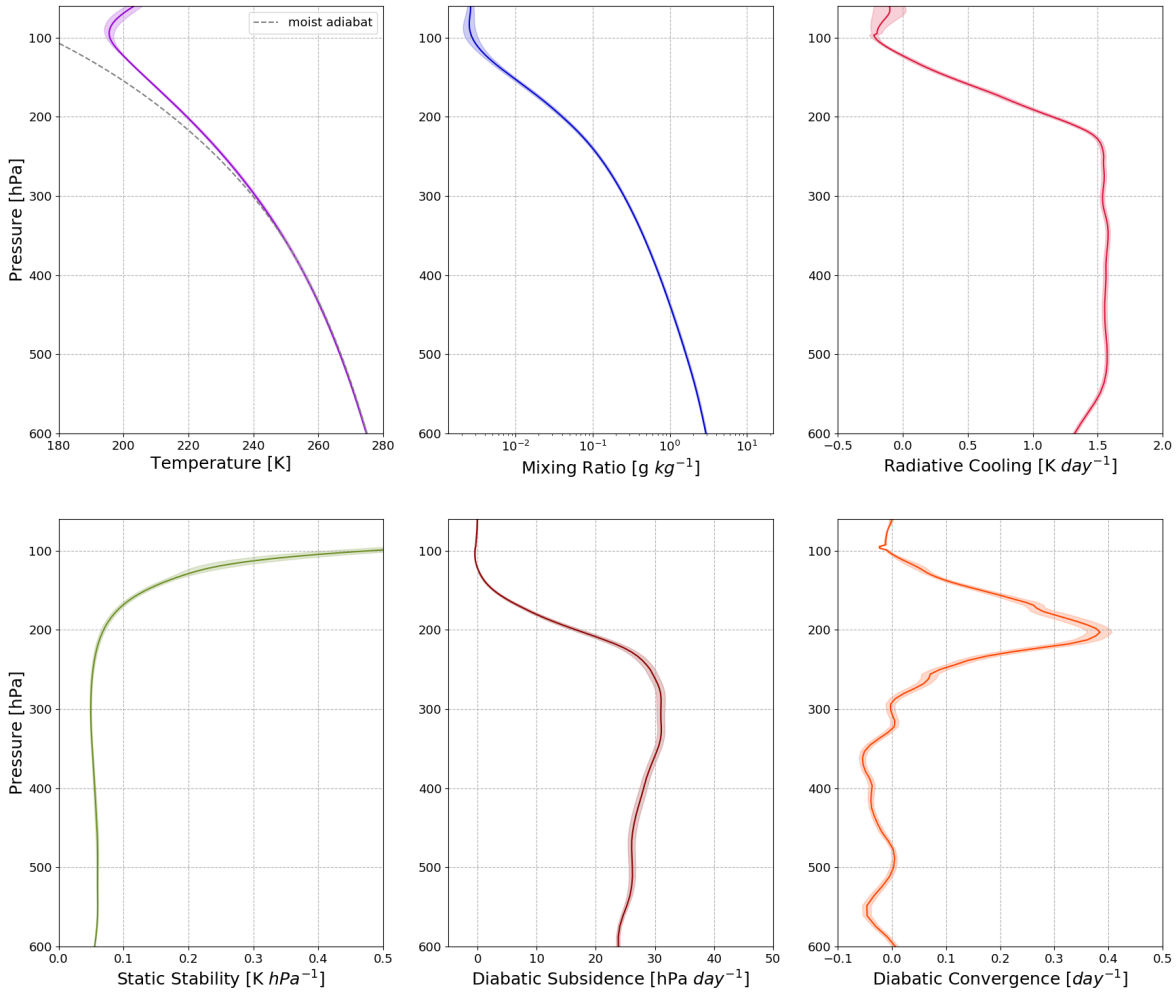

Figure 4.2: Tropical mean temperature (purple), mixing ratio (blue), plotted on logarithmic scale, radiative cooling (red), static stability (green), diabatic subsidence (brown) and diabatic convergence (orange) profiles. The gray dashed line represents the temperature trend of an air parcel moving along the moist adiabat with the starting temperature of $294.5K$ at $1000hPa$. The shaded areas represent the temporal standard deviation of the tropical averages.

First of all, the mean state of the tropical atmosphere is described. The time mean tropical mean profiles of temperature and mixing ratio as well as radiative cooling, static stability, diabatic subsidence and diabatic convergence calculated out of radiative convective equilibrium are shown. All profiles are plotted as functions of pressure in figure 4.2.

Below $300hPa$ the tropical temperature decreases steadily with decreasing pressure following the moist adiabat. Above $300hPa$ the temperature profile becomes more stable than the moist adiabat therefore temperature decreases slower, until reaching a minimum near $100hPa$ marking the beginning of the tropopause. The mixing ratio, plotted on a logarithmic scale, declines exponentially with height due to its fundamental dependency on temperature, reaching its minimum at $100hPa$. Radiative cooling Q_r between $500hPa$ and $280hPa$ is approximately

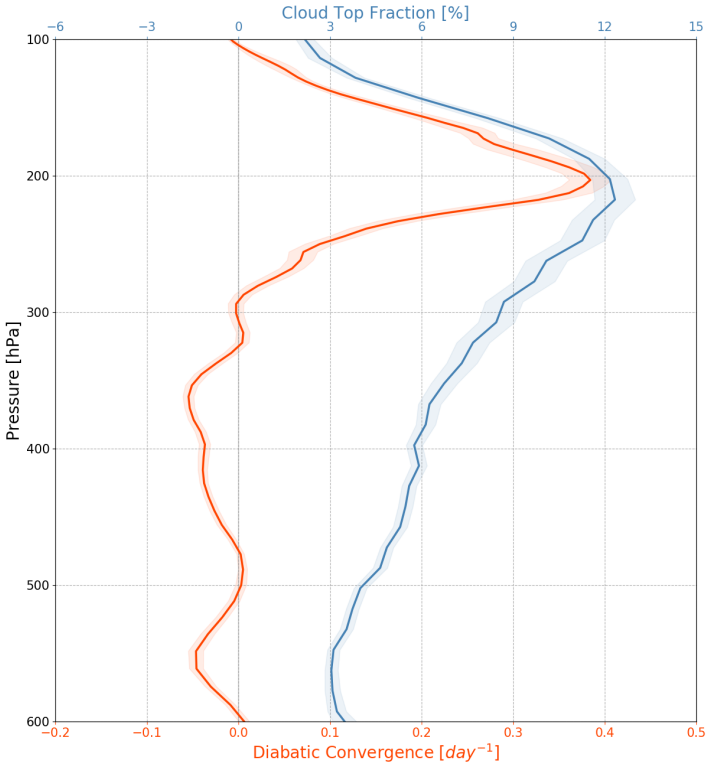

Figure 4.3: The orange curves represent the tropical mean convergence and the blue ones the tropical mean cloud top fraction profile. The shaded areas represent the standard deviation.

constant at $1.5Kday^{-1}$ and above that level it sharply falls to a level of zero radiative cooling. At low enough temperatures in the upper troposphere, water vapour concentrations are so

low that the radiative cooling by water vapour becomes inefficient. This leads to the strong reduction of radiative cooling, since it is dominated by water vapour. Static stability s is nearly constant for the whole troposphere. However, the decline in radiative cooling forces the temperature profile to become increasingly more stable than the moist adiabat, leading to a strong increase of static stability. The rapid decrease in radiative cooling and increase in static stability in the upper troposphere provoke a rapid reduction of diabatic subsidence (ω) above $250hPa$ until it reaches a value of zero, since ω is directly proportional to Q_r and inversely to s (equation 2.4). The subsidence is required to compensate radiative cooling. Below $250hPa$ diabatic subsidence slightly approximately constant. The vertical gradient of diabatic subsidence corresponds to diabatic convergence. Therefore, the convergence is strongest at the point where subsidence decreases most. This generates a peak in convergence at around $200hPa$. The weak zigzag pattern in the convergence profile is caused by small inaccuracies in the interpolated temperature and mixing ratio profiles, which magnify when calculating the convergence profile. The resulting peak at $200hPa$ of the convergence agrees well with the findings of Hartmann and Larson and Zelinka and Hartmann (2010). It marks the maximum height for divergence in the convective regions and thus the net level of convective detrainment. Moreover the detrainment and maximum convergence lie well below the tropopause and therefore do not seem to be directly related to lapse rate changes (Hartmann and Larson, 2002).

Assuming mass continuity the strong convergence in the upper troposphere of the clear-sky region must be mimicked by divergence in the convective regions. This balance leads to the formation of anvil clouds. Therefore the diabatic convergence profile is compared to the cloud top fraction profiles generated with the CLARA-A2 dataset in the upper troposphere (fig. 4.3). The cloud top fraction profile shows a strong peak slightly below $200hPa$, revealing a good, albeit not perfect, agreement in terms of the height level with the convergence peak. This slight deviation to the convergence peak could be caused by the underestimation of the height of thin high clouds by the CLARA-A2 data. The results show the same relationship between the upper tropospheric maximum convergence peak and cloud top fraction peak, as found by Kubar et al. (2007) in MODIS observations, Kuang and Hartmann (2007) and Zelinka and Hartmann (2010) in cloud resolving models and Zelinka and Hartmann (2011) in several satellite datasets. Around $100hPa$ the convergence falls below zero, but cloud top fraction still has a value of 2.5%. This displays the existence of overshooting tops. Overshooting tops occur if a strong updraft in a convective core intrudes its equilibrium level and forms a dome-like structure on top of the anvil clouds. All mean profiles are in good agreement with the theory of the convective radiative equilibrium (Manabe and Strickler (1964)). The diabatic conver-

gence is primarily determined by diabatic convergence which in turn is heavily influenced by water vapour mixing ratio. The resulting peak in convergence corresponds to the anvil height.

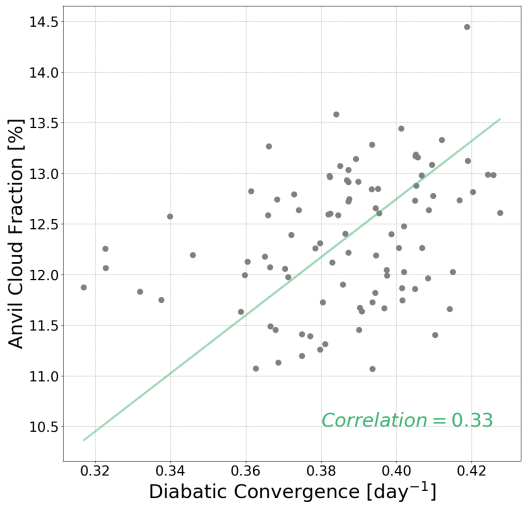

Figure 4.4: Scatter-plot between maximum cloud top fraction and maximum upper tropospheric convergence. The regression slope has a value of 28.7%day.

Figure 4.4 compares monthly mean maximum cloud top fraction with the upper tropospheric maximum convergence. It is shown that there is a weak positive linear correlation between anvil cloud top fraction and maximum convergence. The strong variability in the data inhibits to evaluate a clear correlation between the peaks.

In figure 4.2 profiles calculated by using the tropical mean and monthly means of temperature and specific humidity following the methods by Zelinka and Hartmann (2011) are shown. However, it is also possible to apply the radiative convective equilibrium model konrad to the monthly means of the reanalysis data without performing a spatial average first. With this method, most profiles show merely slight changes in their mean profiles (figure A.1), but it is important to notice that the peak in upper tropospheric convergence shifts up to lower pressures. Hence the height level of the maximum convergence in the upper troposphere is sensitive to way of calculating. This is likely because regional effects are stronger represented with this method, illustrating the influence of the moist convection regions. More moisture leads to enhanced radiative cooling, which in turn is reflected by the shifted profiles of diabatic convergence.

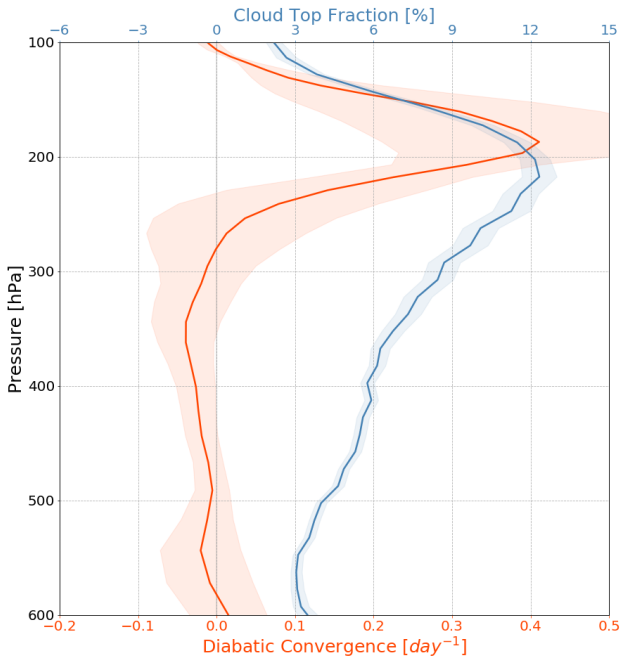

Figure 4.5: The same quantities plotted as in figure 4.3, but new convergence profile. By changing the order of averaging a spatial standard deviations can be calculated.

4.2 Sensitivity to Surface Temperature Changes

To investigate how high clouds react to changes in surface temperature a sensitivity analysis for each profile is performed, following the method of Zelinka and Hartmann (2011). The variability of surface temperature mostly due to ENSO events provides a range of surface temperature changes of $1K$.

For an $1K$ change of surface temperature the whole troposphere below $100hPa$ warms, with a peak warming at around $200hPa$. The mixing ratio mimics the increase of temperature, given by the Clausius-Clapeyron relationship. The mixing ratio profile increases roughly constantly by about 10 $\%K^{-1}$ for all levels below $300hPa$, for lower pressures it maximizes to $25\%K^{-1}$ and then falls of to zero. Since the radiative cooling is mostly determined by water vapour, the radiative cooling imitates the changes in mixing ratio. At pressures less than $200hPa$ the radiative cooling reaches its maximum. This indicates, that the surface warming shifts the decline in radiative cooling towards higher pressure levels, which corresponds with the FAT and PHAT theory. The warming in the troposphere causes a slight increase in static stability and in addition the decline of warming above $200hPa$ as well as the transition to

cooling above $100hPa$, causes a strong reduction in stability. Increasing radiative cooling and static stability induce a reduction of subsidence below $250hPa$. Above that the strong increase in radiative cooling and decrease in stability generate a positive maximum of diabatic subsidence at $200hPa$. The vertical gradient of the diabatic subsidence corresponds to diabatic convergence, hence the maximum convergence declines below and increases above the $200hPa$ subsidence maximum, accounting for an upward shift of the maximum convergence. The weak zigzag pattern again is caused by small inaccuracies in the interpolated temperature and mixing ratio profiles.

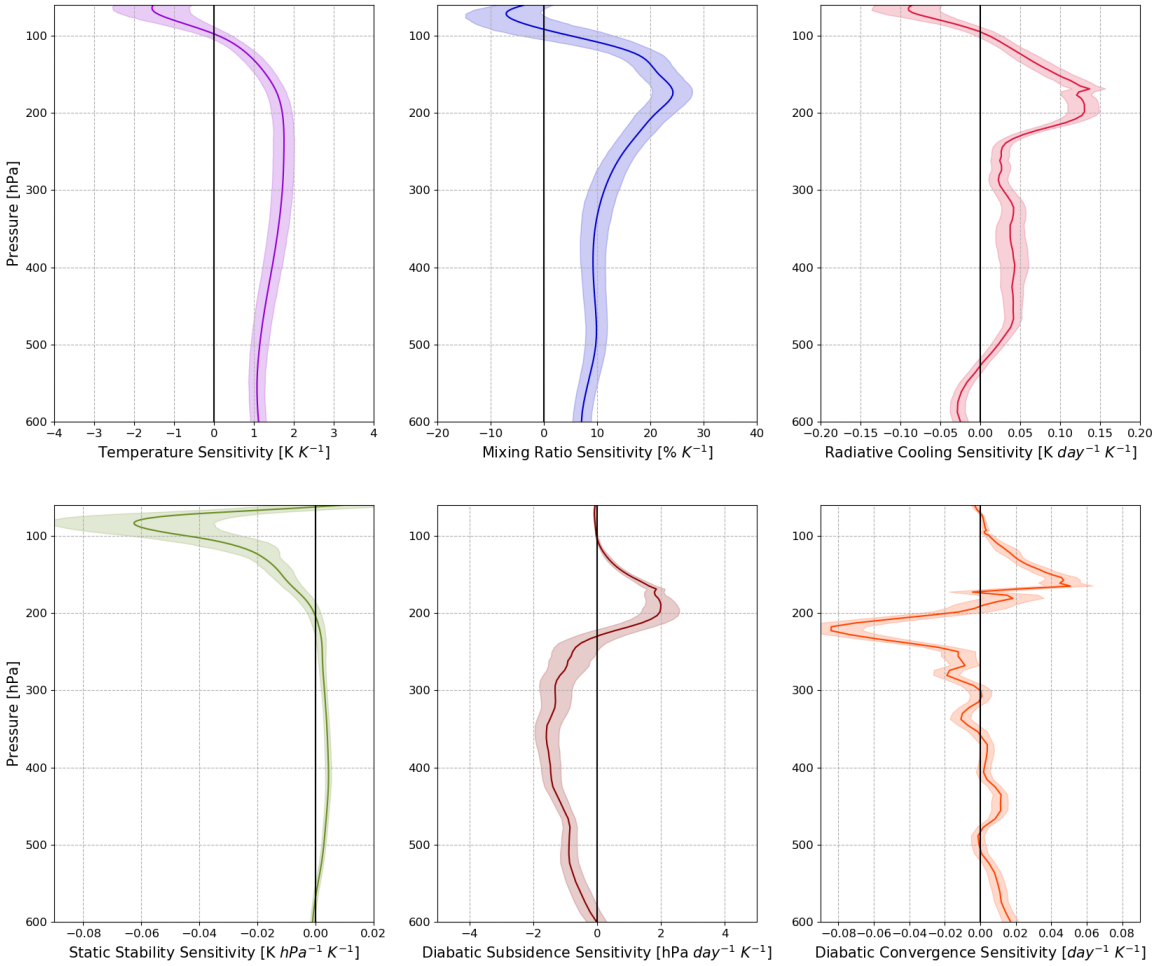

Figure 4.6: Sensitivity analysis results for temperature (purple), mixing ratio (blue), radiative cooling (red), static stability (green), diabatic subsidence (brown) and diabatic convergence (orange). The shaded area represents the 95% confidence interval of the regression coefficient.

The convergence sensitivity profile shows that for a $1K$ surface temperature increase the peak slightly shifts upward and additionally the magnitude of convergence is reduced. These results agree with the findings of Zelinka and Hartmann (2011), although some of the sensitivity profiles show slight deviations.

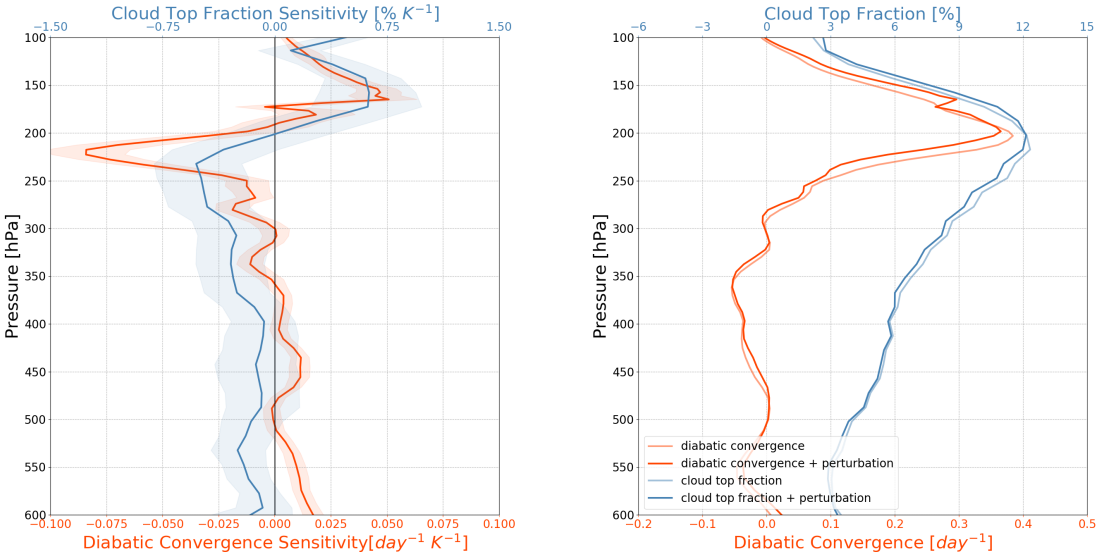

Figure 4.7: (left) Sensitivity of diabatic convergence (orange) and cloud top fraction from CLARA-A2 to the mean surface temperature. (right) mean profiles and sum of mean profiles and perturbations. The perturbations are given by the sensitivity analysis (figure 4.6).

The sensitivity of diabatic convergence and cloud top fraction to surface temperatures are shown in figure 4.7. For positive temperature anomalies, the cloud top fraction profile exhibits an increase between 100 and $200hPa$ and a reduction for pressures below $200hPa$. This is similar to the convergence sensitivity profile. However, the profiles deviate in the strength of the maximum reduction around $250hPa$ and the convergence has a slightly higher location of zero crossing. The resulting convergence and cloud top fraction are plotted together with the initial profiles in the right figure of figure 4.7. Corresponding to an $1K$ increase in surface temperature the convergence profile shows a reduction of $0.0188day^{-1}$ and an upward shift of the convergence peak of about $5hPa$. The cloud top fraction profile exhibits an upward shift of about $15hPa$ and only a minimal reduction of the peak value is noticeable. However the value for the relatively strong upward shift of the anvil peak is induced by the coarse vertical resolution of the profile.

The same comparison was conducted with the convergence profiles, which are calculated using the reanalysis data without performing a spatial average first (figure A.2). The sensitivity of the convergence profile shows the similar behavior as the convergence calculated following the method of (Zelinka and Hartmann, 2011). However, the whole profile again is at slightly higher pressure levels. This is further evidence that the reduction and upward shift of the peak in convergence is a robust result.

In order to assess the degree of agreement of the upward shift in convergence and cloud top fraction, the upper tropospheric convergence weighted pressure is compared to the high cloud weighted pressure (fig. 4.8). The rise of both quantities is not exactly uniform. The monthly upper tropospheric convergence weighted pressure shifts upward of about $7.5hPa$ per Kelvin surface warming (A.3), while the high cloud weighted pressure only shifts upwards with $5hPa$ per Kelvin surface warming (A.4). However only weak correlations found between each compared pair, this again could be caused by the too strong influence of the natural variability in the monthly mean data.

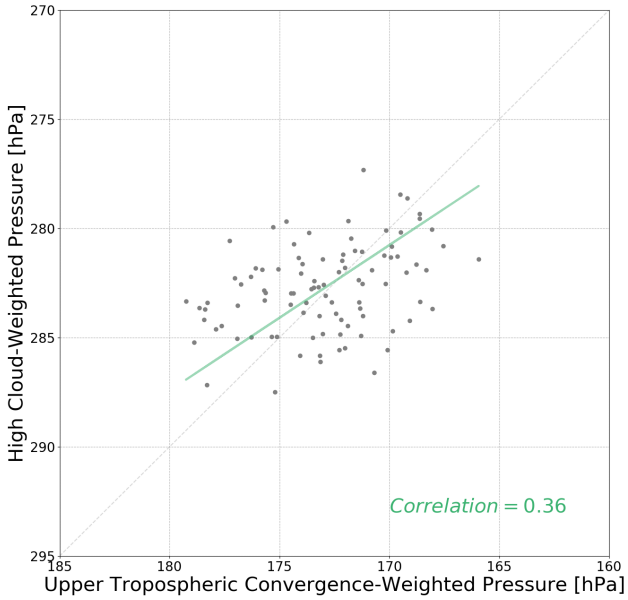

Figure 4.8: High cloud weighted pressure plotted against upper tropospheric convergence weighed pressure. The green line represents the orthogonal distance regression. The dashed line is a 1:1 line, which passes through the mean value of both quantities. The regression slope has a value of $0.66hPa/hPa$

In summary, the results of the sensitivity analysis show an upward shift of the maximum convergence in the upper troposphere as well as the anvil cloud fraction. Furthermore a weak reduction of the convergence maximum is shown, however only a minimal reduction of the anvil cloud amount.

4.2.1 FAT or PHAT?

The fixed anvil temperature and the proportional higher anvil temperature hypothesis both predict that high clouds tend to rise as the climate warms. While the FAT hypothesis predicts an isothermal rise, the PHAT hypothesis states that the cloud tops should in fact slightly warm. The results in this study confirm a rise of the high clouds, along with a vertical displacement of the diabatic convergence profile. Thus, a positive high cloud feedback seems evident from the observations. In order to distinguish whether the shift in convergence and cloud top fraction corresponds to the FAT or PHAT hypothesis, which will determine the strength of the cloud feedback, the most relevant variables are plotted as functions of temperature (4.9), as Zelinka and Hartmann (2011) and Zelinka and Hartmann (2010).

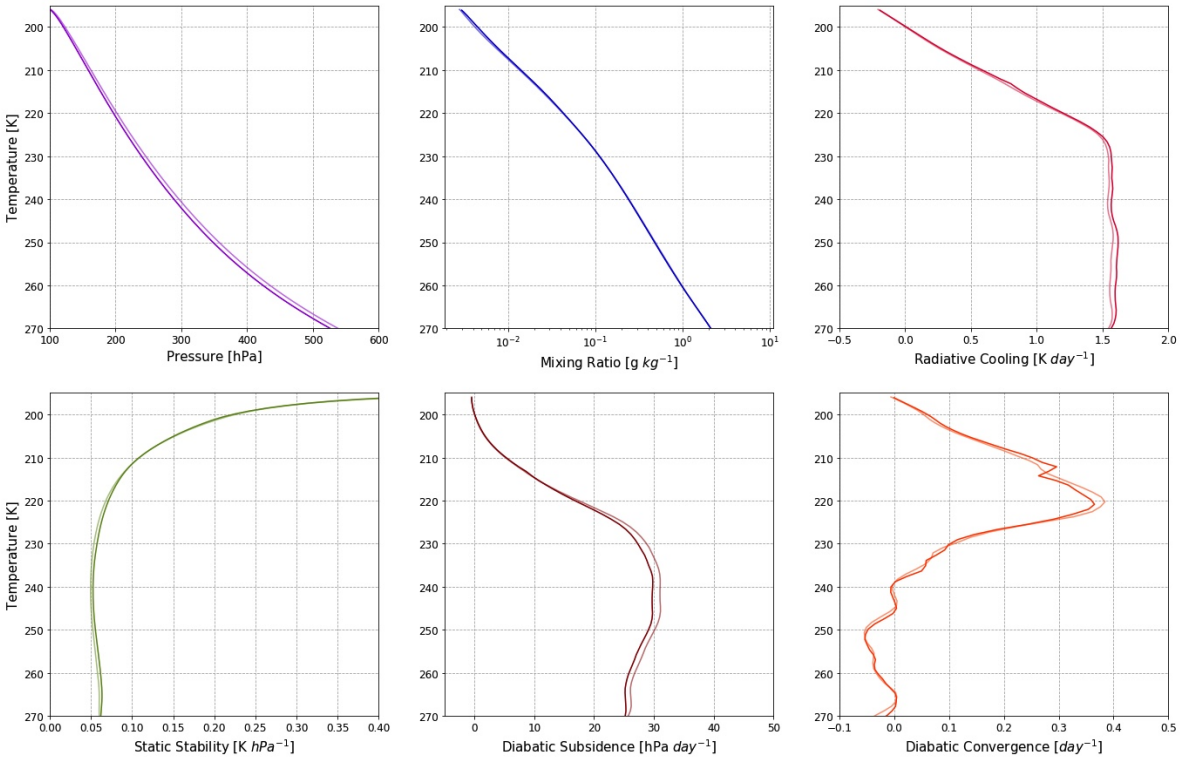

Figure 4.9: Same quantities as in figure 4.2 plotted as functions of temperature. Thin lines are the mean profiles and the thick lines represent the sum of the mean profiles with the perturbation profile. The perturbation profiles are given by the sensitivity analysis (fig. 4.6)

The temperature profile shows a weak warming, while the mixing ratio stays constant due to the exclusive dependency of water vapour to temperature. The radiative cooling slightly increases for temperatures higher $225K$. However, the temperature where radiative cooling drops of stays constant at around $225K$, underlining the fundamental relationship to the Clausius Clapeyron law. The static stability profile very slightly increases for temperatures higher $215K$. The slight increase in stability and radiative cooling cause a reduction of diabatic subsidence. Therefore the peak in convergence reduces and warms by about $0.6K$. This exhibits that the convergence profile not shifts isothermally upwards, which indicates a PHAT-like response for the convergence profile.
These findings overall are in agreement with observational results from Zelinka and Hartmann (2011). In contrast, they substantially differ to the model results from Zelinka and Hartmann (2010), which demonstrates a strong increase in static stability in the upper troposphere and a clear warming of the convergence peak. Zelinka and Hartmann (2011) explained that the difference in stability changes occurs due to the missing upward shift of the ozone profiles in the models of Zelinka and Hartmann (2010). The isothermal shift will likely affect the ozone profiles, which was not taken into account. Therefore the missing upward shift could cause the strong increase of upper tropospheric static stability in the results of (Zelinka and Hartmann, 2010).

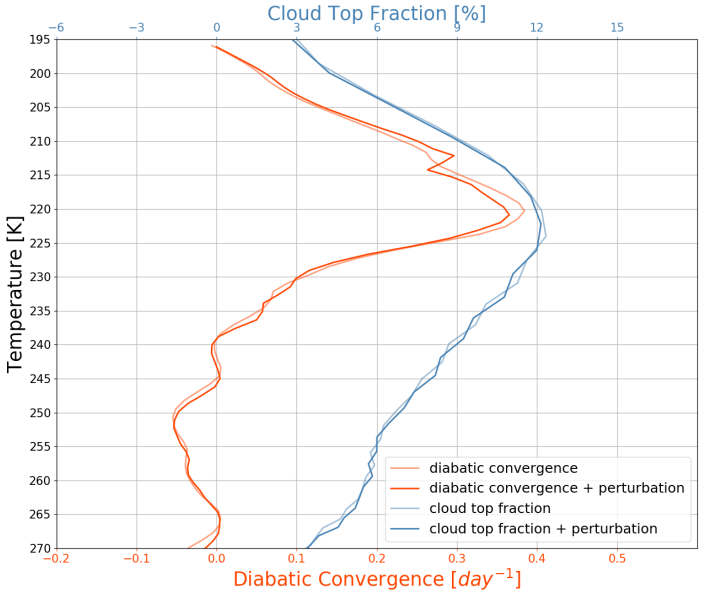

Figure 4.10: Same quantities as plotted in the right figure of figure 4.7 as a function of temperature.

Following the mass balance the peak in cloud top fraction should also shift to slightly warmer temperatures. In figure 4.10 the convergence and cloud top fraction profiles along with their sensitivity to a $1K$ surface temperature warming are displayed. The cloud top fraction shows a shift of $0.02K$ per $1K$ surface warming, compared to a shift of $0.5K$ shown by Zelinka and Hartmann (2010). Therefore, unlike the results for the convergence the cloud top shows no significant shift towards higher temperatures in this study. While the behaviour of clouds and convergence in the study by Zelinka and Hartmann (2011) is more consistent than the results presented here, Zelinka and Hartmann (2011) can also not show a statistically significant shift. The difference in the cloud top pressures between Zelinka and Hartmann (2011) and the study here could be related to the different resolution of the satellite products. The results here imply that a FAT-like respond is more likely.

The results reveal an inconsistent behavior of high cloud and convergence peak. Therefore, the upward shift is investigated in more detail by analysing the correlation of monthly mean peak values and surface temperature in the following section.

Peak Maximum Temperature

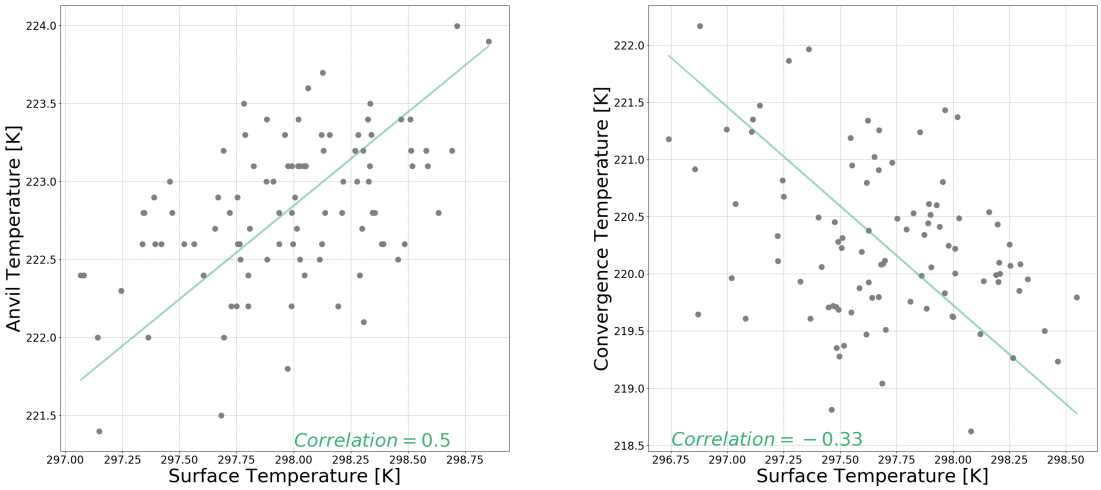

Figure 4.11: (left) Surface temperature plotted against maximum anvil cloud temperature. The corresponding regression slope has a value of $1.19K/K$. (right) Surface temperature versus temperature of maximum upper tropospheric convergence. The regression slop has a value of $-1.73K/K$.

To assess the relationship of the cloud top temperature and convergence at anvil height

with surface temperature the temperatures of the maximum of the peaks are compared to the surface temperatures. However, the resolution of the cloud top fraction is to coarse and the maximum value jumps between two indices (fig. A.5), hence the correct maximum must be located somewhere between two pressure levels. In order to solve this problem the cloud top fraction profile is interpolated on to a finer vertical grid (fig. A.6). This is conducted using the same interpolation method as for the temperature and specific humidity profile. The maximum is picked from the new profile and plotted against the surface temperature.

The results show a shift to warmer temperatures for the anvil temperature of about $1.1K$ per $1K$ surface warming. The maximum convergence in the upper troposphere shows no warming, but a cooling for increasing temperature. This result is contrary to the results before. However the weak correlations found between surface temperature and convergence peak temperature indicates that the is a very uncertain result.

Weighted Temperature

Since the peak maximum temperature method shows no clear results, a different method is tested. The second way of assessing the strength of the temperature shift is by comparing the high cloud-weighted temperature and the upper tropospheric convergence-weighted temperature with surface temperature.

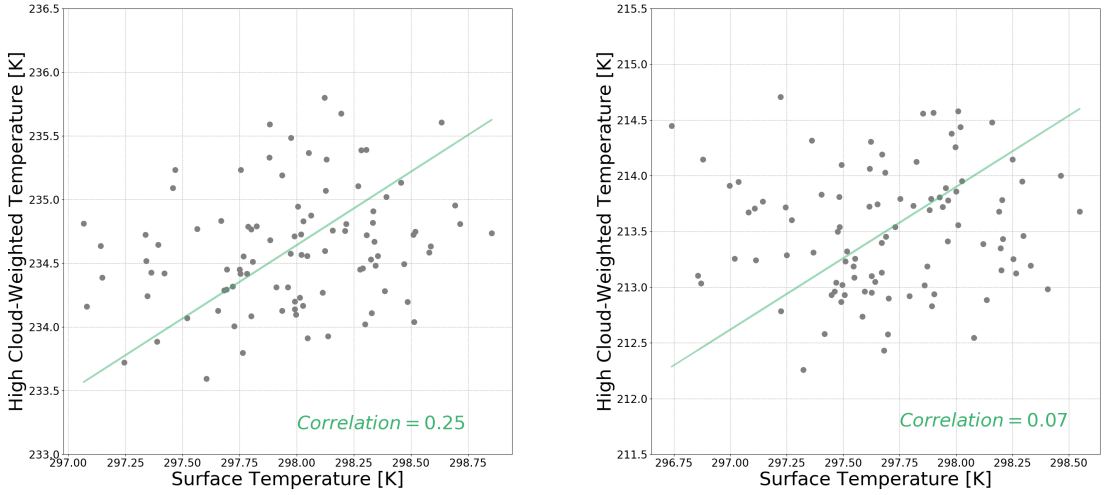

Figure 4.12: (left) Surface temperature plotted against high cloud weighted temperature. The regression corresponding regression slope is $1.15K/K$. (right) Surface temperature versus upper tropospheric convergence weighted temperature, with a value of 1.2 of the regression slope.

Regarding to the regression line the high cloud weighted temperature as well as the upper tropospheric convergence temperature indicate a shift towards warmer temperatures for an increasing surface temperature of about $1.2K$. However, there are only weak correlations found between each quantity and the surface temperature. These results again show no clear correlations, but reveal a likely-hood for a positive correlation, which would indicate a PHAT-like response. Once again the very weak correlations indicate that the results are very uncertain. It could be assumed that the results of Zelinka and Hartmann (2011) might show the same uncertainties.

4.2.2 Stability Iris Effect ?

Bony et al. (2016) demonstrate that an increase in static stability for warmer surface temperatures reduces the convergence and thereby the anvil cloud fraction. Therefore it is investigated in the following, if an increase in stability could be the reason for the reduction in convergence and cloud fraction at anvil height.

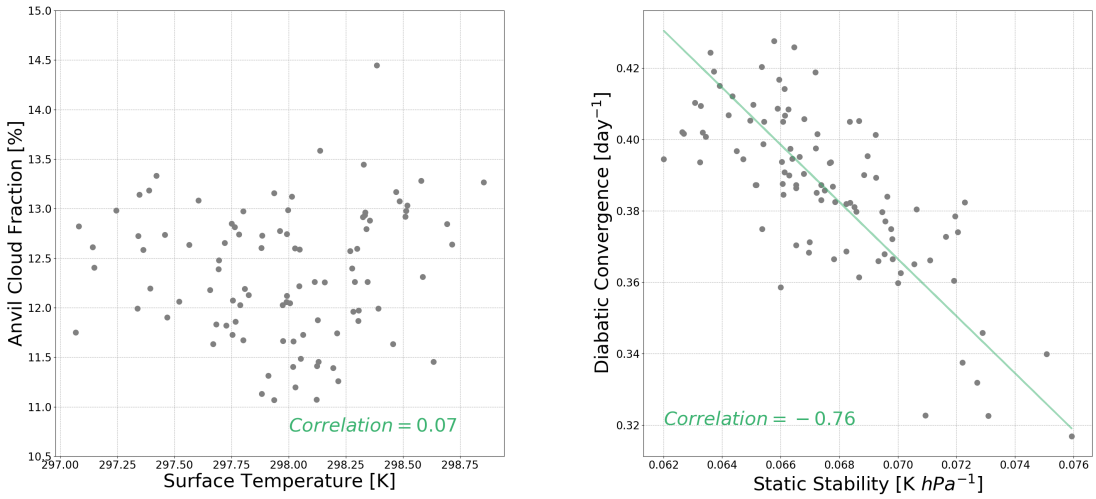

Figure 4.13: (left) Monthly mean tropical anvil cloud fraction plotted against monthly mean tropical surface temperature. (right) Monthly mean tropical static stability plotted against monthly mean tropical convergence at the height of anvil clouds. The corresponding regression slope has a value of $-7.99 day^{-1}\ K^{-1}\ hPa$

Figure 4.4 shows that the anvil cloud amount weakly correlates with the convergence at anvil height. In addition, comparing static stability and diabatic convergence at the height of anvil clouds reveals a clear correlation between them. However, there is no correlation found between monthly mean anvil cloud fraction and surface temperature. The correlation between

convergence and stability as well as convergence and anvil fraction accord with theory of the stability iris hypothesis, but the link between surface temperature and anvil cloud amount is missing. However, the timescales and forcing strength are vastly different to those of Bony et al. (2016). The study by Bony et al. (2016) uses annual means simulated by general circulation models for a 26-year time period. However here monthly means are analysed, hence the natural variability could weaken the correlation between anvil cloud amount and surface temperature. Furthermore the found correlation between static stability and convergence support the theory of PHAT. Zelinka and Hartmann (2010) showed that an increase in static stability is the main reason for a slight warming of the cloud tops, hence this correlation between convergence and stability found here supports this.

5 Summary and Conclusion

In this study the sensitivity of high clouds to changes in surface temperatures was investigated, focusing on three known mechanisms describing the variation of high clouds to surface temperature variability. The first one is the fixed anvil temperature hypothesis (Hartmann and Larson, 2002), which claims that high clouds will rise isothermally as the climate warms, resulting in a positive cloud feedback. In contrast, the proportional higher anvil temperature hypothesis (Zelinka and Hartmann, 2010) shows, that the rising cloud tops will not stay at a fixed temperature, but will slightly warm due to increasing static stability. This still results in a positive cloud feedback, albeit smaller in magnitude. The third mechanism, the iris effect (Bony et al., 2016), describes the horizontal changes of the high clouds induced by warming surface temperatures. An increase in static stability leads to a reduction of the convergence and thereby to a reduction of the anvil cloud fraction. The described mechanisms are widely proven in model based studies, however there is a limited number of observational evidence. The observational study by Zelinka and Hartmann (2011) uses several satellite measurements to consider high cloud changes due to interannual variability of surface temperatures mainly caused by ENSO events. The results are similar to those of studies using climate models and demonstrate that the convergence is a good tool to describe the behavior of high clouds. Hence this study uses a different set of observational data to find observational evidence for changes in high clouds due to surface temperature variations. The methods used are similar as Zelinka and Hartmann (2011) in order to evaluate if the results can be reproduced with a different dataset. In addition, the relationship of convergence and high clouds is investigated more closely.

The tropical mean profiles, which are composed of observations, reanalysis and a radiative convective model, show good agreement to the results of past studies and the theory of convective radiative equilibrium. Looking more closely at the monthly mean peak values indicates a correlation, albeit weak, between maximum cloud top fraction and maximum upper tropospheric convergence. Nevertheless a good agreement of convergence and cloud top fraction in the upper troposphere is found.

A sensitivity analysis to surface temperature variation reveals a reduction as well as a slight upward shift of the maximum convergence. The cloud top fraction shows a similar behaviour, although the reduction of the maximum cloud fraction is weaker. For an increase in $1K$ the

peak in convergence shifts for about $5hPa$ upward and the anvil fraction for about $15hPa$. A comparison of the upward shift with the monthly mean weighted pressures shows that the rise of convergence and cloud top fraction is not uniform. Furthermore a reduction of the convergence peak and a minimal reduction of the cloud top fraction peak is found. The results indicate a high likely-hood for the rise of the convergence maximum and high clouds. The convergence is suitable to describe the upward shift of high clouds, however not the strength of the upward shift. The horizontal variability of high clouds is not well represented by the convergence.

Robustness of the method was tested by changing the calculation method for the convergence profile, calculating the spatial mean only after konrad was used to calculate the convergence. The results demonstrate that the influence of regional effects leads to a slightly higher pressure level of the convergence peak. However, the sensitivity to an $1K$ surface temperature increase are similar. Therefore the height level of the convergence maximum is sensitive to the way of calculating, but the sensitivity analysis not. Leading to the assumption that the methods of Zelinka and Hartmann (2011) for assessing the sensitivity to surface warming are likely robust, but the determination of the pressure level of the convergence maximum in the upper troposphere not.

To answer to question of FAT versus PHAT all relevant variables and their sensitivity to surface warming are illustrated as a function of tropospheric temperature. The radiative cooling slightly increases for warmer surface temperatures, but the temperature where radiative cooling starts declining stays constant. The static stability slightly increases and therefore the convergence profile reduces and shifts to warmer temperature of about $0.6K$. This reduction and upward shift should be mimicked by the cloud top fraction profile. However,this is not the case. The behaviour of the convergence points towards PHAT and is similar to that of Zelinka and Hartmann (2011), however the behaviour of the cloud tops indicate a FAT-like response. To assess this inconsistency the peak maximum temperature-method and weighted temperature-method are used to further investigate the relationships of convergence and cloud tops to the surface temperature. It is shown that the likely-hood of the anvil and convergence peak temperature is not to stay at a fixed temperature, but slightly warm, which would indicate a PHAT-like response. However, the natural variability influences are quite strong leading to weak correlations.

Finally the reduction of the convergence maximum is investigated for agreement with the stability iris hypothesis. The results show a moderate correlation between monthly mean

convergence and static stability at the height of anvil clouds. This agrees with the stability iris hypothesis (Bony et al., 2016), but the link between anvil cloud amount and surface temperature is missing.

While the results of this study point to a PHAT-like response of high clouds and the existence of an iris effect, many of the correlations are weak (see figures 4.4, 4.8, 4.11,4.12 as well as 4.13) and thus the uncertainty is rather large. This needs to be considered when evaluating the results presented here. There are a number of possible reasons for these uncertainties.
While model-based studies are able to look at long timescale with strong forcing, it is only possible to display short timescales for observational studies, due the lack of long-term satellite observational records (Zhou et al., 2015). Therefore only short-term cloud feedback can be illustrated. Dessler (2010) found no correlation between long and short term feedback, however cloud feedback was not precisely tested. The newer study by Zhou et al. (2015) demonstrates that only considering cloud feedback, there is a correlation between short and long term cloud feedback. The vertical structure of the cloud changes are similar, but models with larger long-term cloud feedback show stronger changes compared to short-term cloud feedback due to interannual variability (Zhou et al., 2015). Furthermore the study by Lu et al. (2008) compared warming induced by El Niño with global warming due to increasing CO_2 concentrations. The results demonstrate a similar vertical structure of the warming in the troposphere for both forcings. However the vertical and horizontal strength is weaker for ENSO induced warming Lu et al. (2008). Overall there are strong indicators that the variability of high clouds due to surface temperature changes are comparable to long term changes, but there can be substantial differences. This could explain some of the weak relationships found in this study.
In addition, the vertical resolutions of convergence and cloud profiles are considerably different, masking some of the small changes. Finally the systematic underestimation of high clouds by CLARA-A2 could be problematic for the evaluation of cloud heights.

A possible approach to reduce the uncertainties for this analysis would be to expand the analysed time period. Extending the analysed time scale would allow a more significant comparison of annual means than the 8 year period used in this study. The correlations might improve, increasing the confidence in the results. Since the CLARA-A2 dataset provides a 34-year period of observational data, it could be suited for this. However, for longer timescales there are inconsistencies due to the different satellites, possibly increasing the uncertainties. It is also possible to asses a nearly 20 year time period with the MODIS dataset. Since the CLARA-A2 has limitations regarding high clouds, MODIS or other satellite datasets, which

can better resolve high clouds, may be more suitable for the analysis. Another approach to reduce the uncertainties would be considering a time period with a stronger surface warming. A stronger forcing would allow to better distinguish between natural variability and the surface warming signal. Therefore a clearer result in the sensitivity of high clouds and convergence to surface temperature should appear. While this study hopefully contribute s to the understanding of tropical high cloud feedback, there are many ways in which future studies could expand the observational evidence.

Bibliography

A. Bakhshaii and R. Stull. Saturated pseudoadiabatsa noniterative approximation. *Journal of Applied Meteorology and Climatology*, 52(1):5–15, 2013.

S. Bony, R. Colman, V. M. Kattsov, R. P. Allan, C. S. Bretherton, J.-L. Dufresne, A. Hall, S. Hallegatte, M. M. Holland, W. Ingram, et al. How well do we understand and evaluate climate change feedback processes? *Journal of Climate*, 19(15):3445–3482, 2006.

S. Bony, B. Stevens, D. Coppin, T. Becker, K. A. Reed, A. Voigt, and B. Medeiros. Thermodynamic control of anvil cloud amount. *Proceedings of the National Academy of Sciences*, 113(32):8927–8932, 2016.

E. Borbas and P. MENZEL. Modis atmosphere l2 atmosphere profile product. *NASA MODIS Adaptive Processing System*, 2015.

S. A. Buehler, J. Mendrok, P. Eriksson, A. Perrin, R. Larsson, and O. Lemke. Arts, the atmospheric radiative transfer simulator-version 2.2. *Geoscientific Model Development*, 11 (4):1537–1556, 2018.

J. H. Chae and S. C. Sherwood. Insights into cloud-top height and dynamics from the seasonal cycle of cloud-top heights observed by misr in the west pacific region. *Journal of the Atmospheric Sciences*, 67(1):248–261, 2010.

A. E. Dessler. A determination of the cloud feedback from climate variations over the past decade. *Science*, 330(6010):1523–1527, 2010.

Z. A. Eitzen, K.-M. Xu, and T. Wong. Cloud and radiative characteristics of tropical deep convective systems in extended cloud objects from ceres observations. *Journal of Climate*, 22(22):5983–6000, 2009.

B. E. Harrop and D. L. Hartmann. Testing the role of radiation in determining tropical cloud-top temperature. *Journal of Climate*, 25(17):5731–5747, 2012.

D. L. Hartmann. *Global physical climatology*, volume 103. Newnes, 2015.

D. L. Hartmann. Tropical anvil clouds and climate sensitivity. *Proceedings of the National Academy of Sciences*, 113(32):8897–8899, 2016.

D. L. Hartmann and K. Larson. An important constraint on tropical cloud-climate feedback. *Geophysical Research Letters*, 29(20):12–1, 2002.

D. L. Hartmann and M. L. Michelsen. No evidence for iris. *Bulletin of the American Meteorological Society*, 83(2):249–254, 2002.

H. Hersbach, W. Bell, P. Berrisford, A. Horányi, M.-S. J., J. Nicolas, R. Radu, D. Schepers, A. Simmons, C. Soci, and D. Dee. Global reanalysis: goodbye era-interim, hello era5. pages 17–24, 04 2019. doi: 10.21957/vf291hehd7. URL `https://www.ecmwf.int/node/19027`.

IPCC. *Climate Change 2013: The Physical Science Basis. Contribution of Working Group I to the Fifth Assessment Report of the Intergovernmental Panel on Climate Change*. Cambridge University Press, Cambridge, United Kingdom and New York, NY, USA, 2013. ISBN ISBN 978-1-107-66182-0. doi: 10.1017/CBO9781107415324. URL `www.climatechange2013.org`.

K.-G. Karlsson, T. Hanschmann, M. Stengel, and J. F. Meirink. Algorithm Theoretical Basis Document CM SAF Cloud, Albedo, Radiation data record, AVHRR-based, Edition 2 (CLARA-A2) Cloud Products (level-1 to level-3), Aug. 2016. URL `https://www.cmsaf.eu/SharedDocs/Literatur/document/2016/saf_cm_dwd_atbd_gac_cld_2_3_pdf.pdf?_blob=publicationFile`.

K.-G. Karlsson, K. Anttila, J. Trentmann, M. Stengel, J. F. Meirink, A. Devasthale, T. Hanschmann, S. Kothe, E. Jaaskelainen, J. Sedlar, et al. Clara-a2: the second edition of the cm saf cloud and radiation data record from 34 years of global avhrr data. *Atmospheric Chemistry and Physics*, 17(9):5809–5828, 2017a.

K.-G. Karlsson, J. Seldar, A. Devasthale, M. Stengel, T. Hanschmann, J. F. Meirink, N. Benas, and G.-J. van Zadelhoff. Product user manual: Cm saf cloud, albedo, radiation data record, avhrr-based, edition 2 (clara-a2): Cloud products, Mar. 2017b. URL `https://www.cmsaf.eu/SharedDocs/Literatur/document/201/saf_cm_dwd_pum_gac_cld_2_3_pdf.pdf?_blob=publicationFile`.

L. Kluft and S. Dacie. atmtools/konrad: A radiative-convective equilibrium model for Python, Mar. 2019. URL `https://doi.org/10.5281/zenodo.2597967`.

L. Kluft, S. Dacie, S. A. Buehler, H. Schmidt, and B. Stevens. Re-examining the first climate models: Climate sensitivity of a modern radiative-convective equilibrium model. *Journal of Climate*, (2019), 2019.

Z. Kuang and D. L. Hartmann. Testing the fixed anvil temperature hypothesis in a cloud-resolving model. *Journal of Climate*, 20(10):2051–2057, 2007.

T. L. Kubar, D. L. Hartmann, and R. Wood. Radiative and convective driving of tropical high clouds. *Journal of Climate*, 20(22):5510–5526, 2007.

B. Lin, B. A. Wielicki, L. H. Chambers, Y. Hu, and K.-M. Xu. The iris hypothesis: A negative or positive cloud feedback? *Journal of Climate*, 15(1):3–7, 2002.

R. S. Lindzen, M.-D. Chou, and A. Y. Hou. Does the earth have an adaptive infrared iris? *Bulletin of the American Meteorological Society*, 82(3):417–432, 2001.

K.-N. Liou. *An introduction to atmospheric radiation*, volume 84. Elsevier, 2002.

J. Lu, G. Chen, and D. M. Frierson. Response of the zonal mean atmospheric circulation to el niño versus global warming. *Journal of Climate*, 21(22):5835–5851, 2008.

S. Manabe and R. F. Strickler. Thermal equilibrium of the atmosphere with a convective adjustment. *Journal of the Atmospheric Sciences*, 21(4):361–385, 1964.

T. Mauritsen and B. Stevens. Missing iris effect as a possible cause of muted hydrological change and high climate sensitivity in models. *Nature Geoscience*, 8(5):346, 2015.

E. J. Mlawer, S. J. Taubman, P. D. Brown, M. J. Iacono, and S. A. Clough. Radiative transfer for inhomogeneous atmospheres: Rrtm, a validated correlated-k model for the longwave. *Journal of Geophysical Research: Atmospheres*, 102(D14):16663–16682, 1997.

C. P. Morice, J. J. Kennedy, N. A. Rayner, and P. D. Jones. Quantifying uncertainties in global and regional temperature change using an ensemble of observational estimates: The hadcrut4 data set. *Journal of Geophysical Research: Atmospheres*, 117(D8), 2012.

S. Platnick, M. D. King, S. A. Ackerman, W. P. Menzel, B. A. Baum, J. C. Riédi, and R. A. Frey. The modis cloud products: Algorithms and examples from terra. *IEEE Transactions on Geoscience and Remote Sensing*, 41(2):459–473, 2003.

C.-D. Schönwiese. *Klimatologie*. UTB, 2008.

D. W. Thompson, S. Bony, and Y. Li. Thermodynamic constraint on the depth of the global tropospheric circulation. *Proceedings of the National Academy of Sciences*, 114(31):8181–8186, 2017.

K. E. Trenberth. The definition of el nino. *Bulletin of the American Meteorological Society*, 78(12):2771–2778, 1997.

K.-M. Xu, T. Wong, B. A. Wielicki, L. Parker, and Z. A. Eitzen. Statistical analyses of satellite cloud object data from ceres. part i: Methodology and preliminary results of the 1998 el niño/2000 la niña. *Journal of climate*, 18(13):2497–2514, 2005.

K.-M. Xu, T. Wong, B. A. Wielicki, L. Parker, B. Lin, Z. A. Eitzen, and M. Branson. Statistical analyses of satellite cloud object data from ceres. part ii: Tropical convective cloud objects during 1998 el niño and evidence for supporting the fixed anvil temperature hypothesis. *Journal of climate*, 20(5):819–842, 2007.

M. D. Zelinka and D. L. Hartmann. Why is longwave cloud feedback positive? *Journal of Geophysical Research: Atmospheres*, 115(D16), 2010.

M. D. Zelinka and D. L. Hartmann. The observed sensitivity of high clouds to mean surface temperature anomalies in the tropics. *Journal of Geophysical Research: Atmospheres*, 116 (D23), 2011.

C. Zhou, M. D. Zelinka, A. E. Dessler, and S. A. Klein. The relationship between interannual and long-term cloud feedbacks. *Geophysical Research Letters*, 42(23):10–463, 2015.

Acknowledgments

First of all I would like to thank Stefan Bühler. He proposed working on the project at hand, guided me through the project and gave me valuable feedback on scientific issues from which I have learned a lot. Furthermore, I would like to thank Akos Horvath for being my second supervisor, taking the time to engage with my project and helping with technical issues. I also want to thank Lukas Kluft for helping me setting up his model konrad and for other useful programming tips as well as Oliver Lemke for his technical support. For valuable comments on my written thesis I would like to thank Christopher Sauter and especially Paul Keil. Thanks also go to Anna Ludwig for fantastic support during the final writing days. Finally, I would like to thank again Paul Keil for showing so much patience with me and for his good scientific advises.

Versicherung an Eides statt

Hiermit versichere ich an Eides statt, dass ich die vorliegende Arbeit im Studiengang M.Sc. Meteorologie selbstständig verfasst und keine anderen als die angegebenen Hilfsmittel insbesondere keine im Quellenverzeichnis nicht benannten Internet-Quellen benutzt habe. Alle Stellen, die wörtlich oder sinngemäßaus Veröffentlichungen entnommen wurden, sind als solche kenntlich gemacht. Ich versichere weiterhin, dass ich die Arbeit vorher nicht in einem anderen Prüfungsverfahren eingereicht habe und die eingereichte schriftliche Fassung der auf dem elektronischen Speichermedium entspricht. Des Weiteren bin ich damit einverstanden, dass meine Arbeit in der Fachbibliothek ausgestellt wird.

Ort und Datum	Unterschrift (Friederike Bär)

Appendix

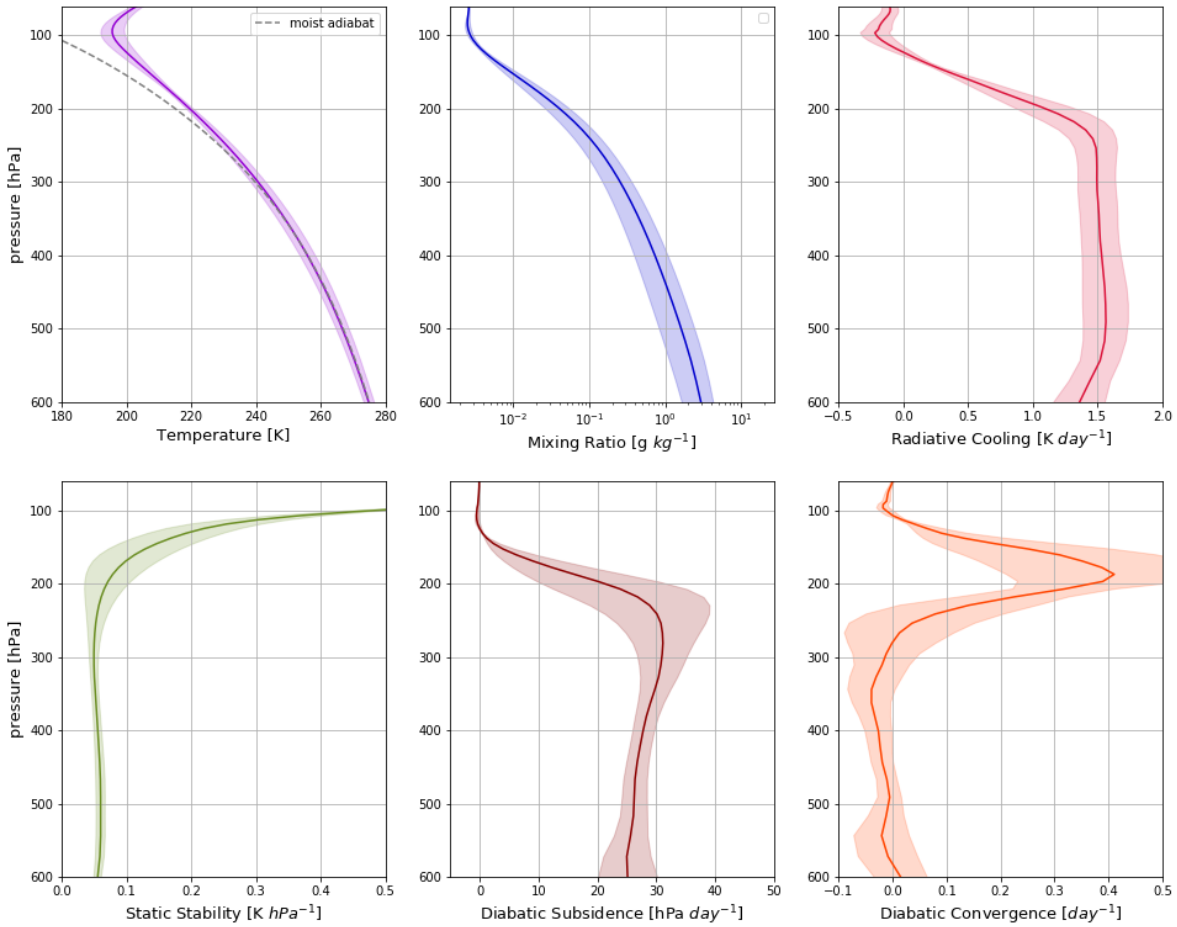

Figure A.1: Same plot as figure 4.2, but the spatial mean calculated only after konrad was used to calculate the convergence.

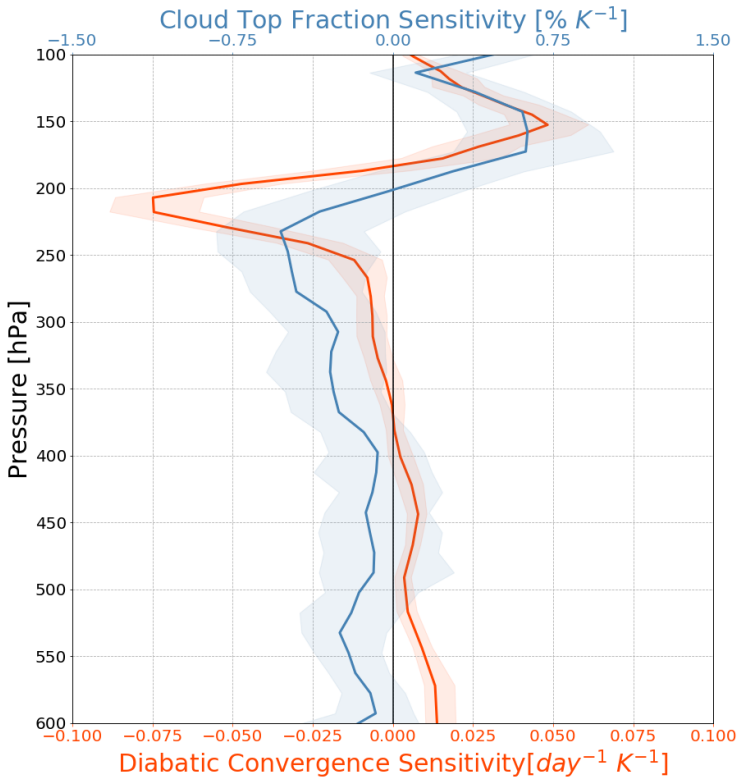

Figure A.2: Same plot as figure 4.2, but quantities used for sensitivity analysis same as in figure A.1.

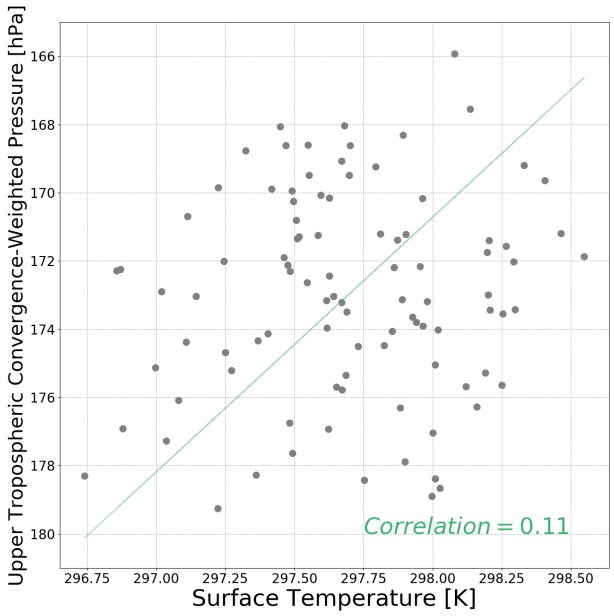

Figure A.3: Surface temperature plotted against upper tropospheric convergence-weighted pressure. The regression slope has a value of $7.5hPa\ K^{-1}$.

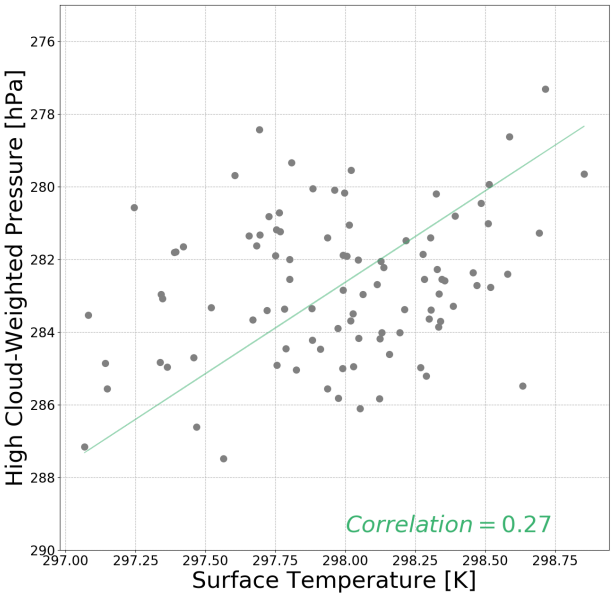

Figure A.4: Surface temperature plotted against high cloud weighted pressure. The regression slope has a value of $5hPa\ K^{-1}$.

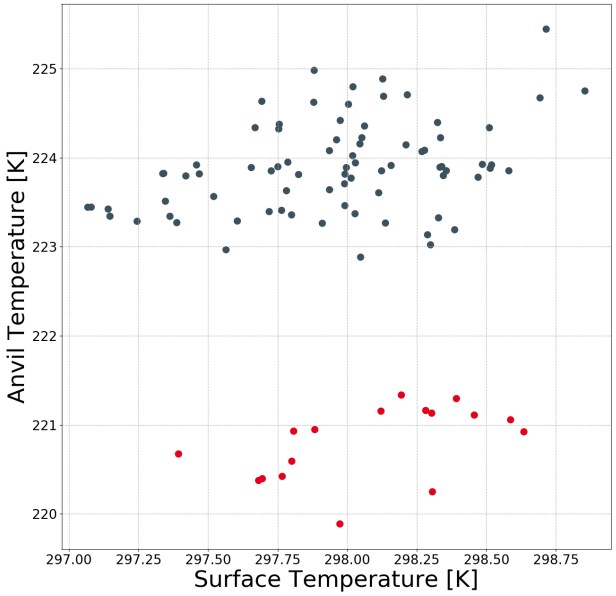

Figure A.5: Surface temperature plotted against anvil temperature. The blue dots represent the maximum values at index 7 of the vertical anvil temperature vector and the red dots index 8.

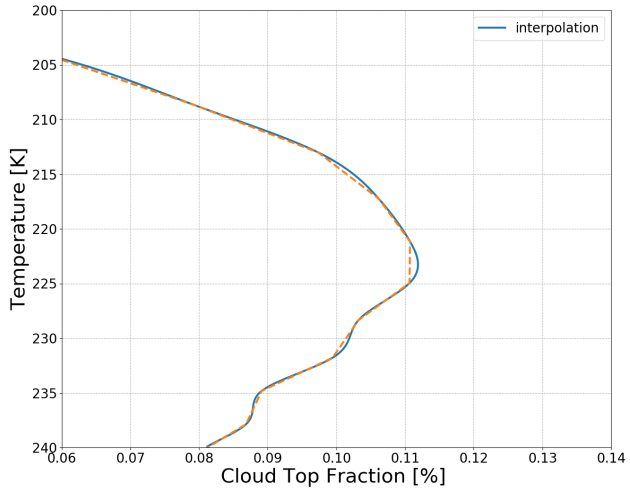

Figure A.6: The orange dotted line represents the cloud top fraction profile and the blue line the interpolated cloud top fraction profile plotted in temperature coordinates.